Russian Chemical Reviews **74** (7) 619 – 637 (2005) © 2005 Russian Academy of Sciences and Turpion Ltd

DOI 10.1070/RC2005v074n07ABEH000911

Pulsed EPR structural studies in the nanometre range of distances

S A Dzuba

Contents

I.	Introduction	619
II.	The EPR spectrum of a radical pair	620
III.	Experimental methods based on electron spin echo envelope modulation	622
IV.	Experimental methods based on spin relaxation	627
V.	Conformations of long-chain biradicals and doubly spin-labelled and metal-containing biomolecules	629
VI.	Cluster nanostructures	630
VII.	Stable paramagnetic pairs in photosynthetic reaction centres of plants and bacteria	632
VIII.	Photoinduced spin-correlated pairs in photosynthetic reaction centres of plants and bacteria	633
IX.	Conclusion	635

Abstract. The possibilities of investigations of the nanostructure of matter by pulsed EPR spectroscopy based on the measurement of the dipole – dipole coupling between the spins of unpaired electrons are considered. Using these methods, one can determine the conformations of long-chain organic biradicals and biomolecules (either doubly spin-labelled or containing paramagnetic metal ions) and study the supramolecular structure of matter, *i.e.*, peptide clustering, heterogeneity of polymer packing, structural details of photosynthetic reaction centres and other complex systems. Investigations of the photoinduced spin-correlated radical pairs also reveal the regularities of charge transfer in these systems. The methods are characterised by high accuracy of measurements (0.03 nm) and can be used for measuring distances in the 1.5 – 10 nm range. The bibliography includes 148 references.

I. Introduction

Research on the structure of matter in the nanometre range of distances (1 – 10 nm or 10 – 100 Å) is necessary for the determination of biomolecule conformations, elucidation of the nanostructure of other complex molecular systems and solution to various problems of supramolecular chemistry. If a system under study is crystallisable, good results can be obtained using conventional X-ray crystallography.[1] Two-dimensional crystals are studied by electron crystallography[2] or scanning tunnelling microscopy.[3] Multidimensional NMR spectroscopy allows the structure of biomolecules of mass up to 100 kDa to be determined.[4] As for disordered media, objects with sizes ranging between 5 and 100 nm are studied by small-angle X-ray scattering (SAXS)[5] and small-angle neutron scattering (SANS).[6] Resonant fluorescence energy transfer is used to determine distances between chromophores in the range from 1 to 10 nm.[7]

If a system contains paramagnetic centres (*e.g.*, free radicals and ions), distances between them can be measured by EPR spectroscopy. The use of this method is based on studies of the dipole – dipole (d – d) interaction between electron spins. Knowing the distances between paramagnetic centres in pairs or clusters (many biomolecules contain paramagnetic metal ions), it is possible to determine certain parameters of the supramolecular structure. Often, physicochemical and biophysical studies are carried out by the spin label and spin probe techniques, which involve introduction of paramagnetic centres into the system under study. Pairs of paramagnetic centres can also appear as a result of charge separation in photosynthesis, which involves formation of radical anion-radical cation pairs.

The dipole – dipole interaction between electron spins in a pair of paramagnetic centres is characterised by the parameter

$$\frac{\mu_0}{4\pi}\frac{g_e^2\beta^2}{r^3},$$

where μ_0 is the magnetic permeability of vacuum, g_e is the g-factor of free electron, β is the Bohr magneton and r is the distance between the paramagnetic centres in the pair. Continuous-wave EPR spectroscopy is used for measuring distances in a pair of electron spins up to 1 – 1.5 nm range.[8] This limit is due to a masking effect of inhomogeneous broadening of the EPR lines owing to unresolved hyperfine coupling with the nuclei of the matrix, which can be as high as $\sim$0.5 mT for organic media.

Pulsed EPR methods based on electron spin echo (ESE) spectroscopy[9,10] are much more sensitive to the dipole – dipole interactions. When using such methods, the dipole – dipole interaction must be compared with the homogeneous broadening, which is much smaller ($\sim$0.01 mT) for organic media. From here the upper boundary of the measured distances is $\sim$5 – 10 nm. The lower boundary (about 1.5 nm) is governed by the temporal resolution of the instrument ($\sim 10^{-8}$ s). In this review we summarise the results obtained by ESE spectroscopy for long-chain organic biradicals and radical pairs in solids. The distances between paramagnetic centres in the systems under study lie between $\sim$2 to 8 nm.

An advantage of ESE spectroscopy is a high accuracy of measurements in this range of distances. For instance, for $r \sim$ 3 nm the error may be only $\sim$0.03 nm. High resolution of the method allows one to reveal some fine details in the nanostructure of matter, which cannot be detected by other methods. Besides, ESE studies do not require a specific sample preparation procedure (*e.g.*, crystallisation, high degree of purification, *etc.*).

S A Dzuba Institute of Chemical Kinetics and Combustion, Siberian Branch of the Russian Academy of Sciences, ul. Institutskaya 3, 630090 Novosibirsk, Russian Federation. Fax (7-3833) 30 73 50, tel. (7-3833) 33 12 76, e-mail: dzuba@ns.kinetics.nsc.ru

Received 19 February 2004
Uspekhi Khimii **74** (7) 686 – 706 (2005); translated by A M Raevskiy

The possibility of using ESE spectroscopy in studies of pairs of paramagnetic centres has long been established. A study of $SO_4^- \cdots SO_4^-$ pairs stabilised in a UV irradiated $H_2S_2O_8$ single crystal was reported in 1969.[11] Small width of the EPR spectrum (the possibility of excitation by MW pulses), the absence of magnetic nuclei and spatial orientation of pairs created prerequisites for successful determination of the distances in the pairs by conventional two-pulse ESE spectroscopy. However, the method appeared to be inappropriate for analysis of free radicals in polyoriented organic systems due to large linewidth in the EPR spectrum, masking effect of electron – nuclear interactions and the 'dead' time problem. Other experimental techniques were developed later, in particular, the Pulsed Electron – Electron Double Resonance (PELDOR),[12,13] the '2 + 1' (see Ref. 14) and double-quantum coherence[15,16] methods as well as approaches based on solid-state NMR pulse sequences.[17] A conventional two-pulse method permits investigations of spin-correlated radical pairs in photosynthetic reaction centres.[18] Here, it is possible to eliminate the problems characteristic of polyoriented organic systems (see above).[19] The effects of partner spin relaxation in a radical – metal ion pair were first reported in Ref. 19. Later the procedure was essentially modified[20] (relaxation probe method). The relaxation effects were also used in the selective hole 'burning' technique[21] and dipolar relaxation-induced modulation enhancement.[22]

At present, ESE spectroscopy is widely used in studies of the nanostructure of complex molecular systems. Thermally equilibrated radical pairs and biradicals are most often studied by the PELDOR method while spin-correlated radical pairs are investigated by the two-pulse echo technique. A large number of reviews on current research are available (see, *e.g.*, Refs 23 – 35), most of them being published recently. The aim of this review is to describe (i) all ESE spectroscopy-based methods of analysis of the nanometre range of distances and (ii) systems studied by these methods.

II. The EPR spectrum of a radical pair

Biradicals and radical pairs differ from one another in the presence or absence of covalent bonds between paramagnetic fragments, respectively. For magnetic resonance, this difference is insignificant; therefore, in the text below we will use the term 'a radical (or paramagnetic) pair' (RP) except for the cases where we deal with particular chemical structures.

1. The spin Hamiltonian of a radical pair

The magnetic dipole – dipole interaction between the magnetic moments of electrons is the main interaction in long-chain biradicals and RPs. The classical expression for the energy of two interacting dipoles has the form

$$E_{\mathrm{d}} = \frac{\mu_0}{4\pi} \frac{r^2 \boldsymbol{\mu}_1 \boldsymbol{\mu}_2 - (\boldsymbol{\mu}_1 \boldsymbol{r})(\boldsymbol{\mu}_2 \boldsymbol{r})}{r^5}, \qquad (1)$$

where $\boldsymbol{r}$ is the radius vector connecting two particles with the dipole moments $\boldsymbol{\mu}_1$ and $\boldsymbol{\mu}_2$, respectively.

The energy of two dipoles with the same spatial orientation is given by

$$E_{\mathrm{d}} = \frac{\mu_0}{4\pi} \frac{\mu_1 \mu_2}{r^3} (1 - 3\cos^2\theta), \qquad (2)$$

where θ is the angle between the direction of the dipole axis and the radius vector $\boldsymbol{r}$.

In quantum mechanics, expression (1) is replaced by the Hamiltonian

$$H_{\mathrm{d}} = \frac{\mu_0}{4\pi} g_1 g_2 \beta^2 \frac{r^2 \boldsymbol{S}_1 \boldsymbol{S}_2 - (\boldsymbol{S}_1 \boldsymbol{r})(\boldsymbol{S}_2 \boldsymbol{r})}{r^5}, \qquad (3)$$

where g_1 and g_2 are the g-factors of particles 1 and 2, respectively, and $\boldsymbol{S}_1$ and $\boldsymbol{S}_2$ are the spin operators of these particles.

The systems considered in this review are characterised by long spin – spin separations and weak exchange interaction, which can be ignored.

The wave functions of unpaired electrons are distributed in space; for some molecules, the distributions can be rather broad. Nevertheless, here on we will always use the point dipole approximation, which assumes that the whole spin density of unpaired electrons is localised at a point. This is a reasonable approximation in all practically valuable cases (see below).

In the framework of yet another approximation the electron – electron dipole – dipole interaction will be considered small compared to the Zeeman interaction between electron spins and the magnetic field, *i.e.*

$$\frac{\mu_0}{4\pi} \frac{g_{\mathrm{e}} \beta}{r^3} \ll B_0 ,$$

where B_0 is the magnetic field strength. This approximation *a priori* holds for the distances in RPs considered in this review; therefore, we can use the perturbation theory assuming that Hamiltonian (3) is small compared to the Hamiltonian of the Zeeman interaction. Expression (3) can be essentially simplified if we neglect the components with zero contributions in the first-order perturbation theory. Expression (3) written in spherical coordinates with the Z axis parallel to the magnetic field direction takes the form

$$H_{\mathrm{d}} = \frac{\mu_0}{4\pi} \frac{g_1 g_2 \beta^2}{r^3} (1 - 3\cos^2\theta) \left[S_{1z} S_{2z} - \frac{1}{4} (S_{1+} S_{2-} + S_{1-} S_{2+}) \right]. \qquad (4)$$

Here we used the projections of the spin operators on the Z axis and the raising – lowering operators.

Relationship (4) is analogous to expression (2), but this analogy is incomplete, because the terms containing the raising – lowering operators have no classical analogues (they reflect the particle identity). The matrix elements involving these operators become significant only if the g-factors of two electrons are similar, so that the Zeeman energy difference $|g_1 - g_2|\beta B_0$ becomes comparable with the energy of the dipole – dipole interaction. This is the case for strong spin – spin coupling (or the equivalent spin approximation). If

$$\frac{\mu_0}{4\pi} \frac{g_{\mathrm{e}}^2 \beta^2}{r^3} \ll |g_1 - g_2| \beta B_0 ,$$

the coupling is weak (inequivalent spins). Note that this review concerns weakly coupled systems only.

The Hamiltonian (4) can be re-written using the total spin operator $\boldsymbol{S} = \boldsymbol{S}_1 + \boldsymbol{S}_2$,

$$H_{\mathrm{d}} = \frac{\mu_0}{4\pi} \frac{g_1 g_2 \beta^2}{4r^3} (1 - 3\cos^2\theta)(3S_z^2 - \boldsymbol{S}^2). \qquad (5)$$

2. Energy levels and the EPR spectrum of a radical pair in magnetic field

Consider a radical pair comprising two radicals with different g-factors. The Hamiltonian of the RP in magnetic field, written in frequency units, has the form

$$\frac{H}{\hbar} = \omega_1 S_{1z} + \omega_2 S_{2z} + \frac{1}{4} \varepsilon_{\mathrm{d}} (3S_z^2 - \boldsymbol{S}^2), \qquad (6)$$

where ω_1 and ω_2 are the resonance frequencies of two radicals in the absence of the dipole – dipole interaction and ε_{d} is the magnitude of the dipole – dipole interaction

$$\varepsilon_{\mathrm{d}} = \frac{\mu_0}{4\pi} \frac{g_1 g_2 \beta^2}{r^3 \hbar} (1 - 3\cos^2\theta).$$

We will write the solution to the Hamiltonian (6) using the wave functions of the triplet

$$|T_+\rangle = |\alpha\alpha\rangle,$$
$$|T_0\rangle = \frac{1}{\sqrt{2}}(|\alpha\beta\rangle + |\beta\alpha\rangle),$$
$$|T_-\rangle = |\beta\beta\rangle$$

and singlet

$$|S\rangle = \frac{1}{\sqrt{2}}(|\alpha\beta\rangle - |\beta\alpha\rangle),$$

states of the RP (α and β are the electron spin projections)

$$|1\rangle = |T_+\rangle, \quad (7)$$
$$|2\rangle = \cos\phi|S\rangle + \sin\phi|T_0\rangle,$$
$$|3\rangle = -\sin\phi|S\rangle + \cos\phi|T_0\rangle,$$
$$|4\rangle = |T_-\rangle,$$

where

$$\tan 2\phi = \frac{2\Delta\omega}{\varepsilon_d}, \Delta\omega = \omega_1 - \omega_2.$$

Note that for weak coupling $\phi \approx \pi/4$, and the wave functions $|2\rangle$ and $|3\rangle$ are transformed into $|\alpha\beta\rangle$ and $|\beta\alpha\rangle$, respectively. The energy levels are shown in Fig. 1 and the energies are given by

$$E_1 = \frac{1}{2}(\omega_1 + \omega_2) + \frac{1}{4}\varepsilon_d, \quad (8)$$
$$E_2 = -\frac{1}{4}\varepsilon_d + \frac{1}{4}\sqrt{\varepsilon_d^2 + 4(\Delta\omega)^2},$$
$$E_3 = -\frac{1}{4}\varepsilon_d - \frac{1}{4}\sqrt{\varepsilon_d^2 + 4(\Delta\omega)^2},$$
$$E_4 = -\frac{1}{2}(\omega_1 + \omega_2) + \frac{1}{4}\varepsilon_d.$$

The expressions for six possible energy differences are as follows

$$E_{12} = \frac{1}{2}(\omega_1 + \omega_2) + \frac{1}{2}\varepsilon_d - \frac{1}{4}\sqrt{\varepsilon_d^2 + 4(\Delta\omega)^2}, \quad (9)$$
$$E_{13} = \frac{1}{2}(\omega_1 + \omega_2) + \frac{1}{2}\varepsilon_d + \frac{1}{4}\sqrt{\varepsilon_d^2 + 4(\Delta\omega)^2},$$
$$E_{24} = \frac{1}{2}(\omega_1 + \omega_2) - \frac{1}{2}\varepsilon_d + \frac{1}{4}\sqrt{\varepsilon_d^2 + 4(\Delta\omega)^2},$$
$$E_{34} = \frac{1}{2}(\omega_1 + \omega_2) - \frac{1}{2}\varepsilon_d - \frac{1}{4}\sqrt{\varepsilon_d^2 + 4(\Delta\omega)^2},$$
$$E_{14} = \omega_1 + \omega_2,$$
$$E_{23} = \frac{1}{2}\sqrt{\varepsilon_d^2 + 4(\Delta\omega)^2}.$$

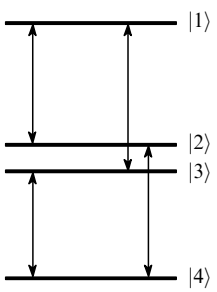


Figure 1. Schematic view of spin energy levels of a radical pair (biradical) in magnetic field.
Shown are the resolved EPR transitions.

The first four differences correspond to the allowed single-quantum transitions (see Fig. 1) and the last two differences correspond to the forbidden two-quantum and zero-quantum transitions.

According to relationships (7), for a thermally equilibrated system the allowed transition intensities are determined by the $\sin^2\phi$ or $\cos^2\phi$ factors because only the matrix elements between the triplet states differ from zero. Thus, the EPR spectrum of a radical pair consists of two doublets with a splitting of ε_d in each (Fig. 2 *a*). In weakly coupled systems, all lines have the same intensities.

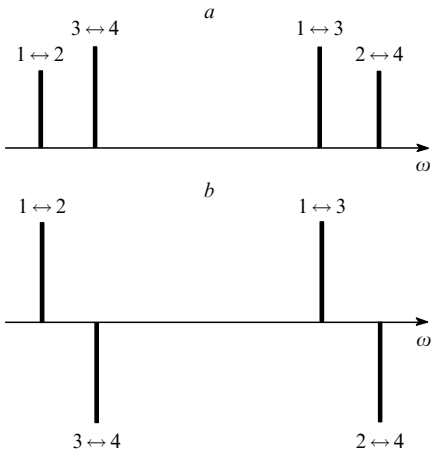


Figure 2. EPR spectrum of thermally equilibrated radical pair (*a*) and spin-correlated radical pair (*b*).

The EPR spectrum of a spin-correlated RP produced from an initial singlet state is shown in Fig. 2 *b*. Such spin-correlated RPs are considered in more detail in Section III.

As will be shown below, all ESE methods are characterised by temporal dependences of the $\cos\varepsilon_d t$ type for thermally equilibrated RPs and of the $\sin\varepsilon_d t$ type for spin-correlated RPs. The Fourier transformation of such dependences creates a doublet at frequencies $\pm\varepsilon_d$ in the EPR spectra. The doublet is symmetrical with respect to zero frequency for thermally equilibrated RPs and antisymmetrical for spin-correlated RPs. By analogy with solid-state NMR spectra this doublet is often called the Pake doublet. However, this is an incomplete analogy, because in NMR we always deal with strong coupling and the splitting in the doublet is $(3/2)\varepsilon_d$. In our case the total splitting in the doublet is $2\varepsilon_d$,† and we will call this doublet the dipolar doublet.

3. Dipolar doublet in polyoriented system

For a polyoriented system the dependence of the line intensities of the dipolar doublet in the EPR spectra of an RP on the frequency ω can be determined by averaging over all spatial orientations of the RP

$$f(\omega) = \frac{1}{4\pi}\int_0^{\pi} d\theta \sin\theta \int_0^{2\pi} \frac{1}{2} d\varphi \left[\delta(\omega - \varepsilon_d) \pm \delta(\omega + \varepsilon_d)\right] \propto \quad (10)$$
$$\propto \left(1 - \frac{4\pi}{\mu_0}\frac{r^3\hbar}{g_1 g_2 \beta^2}\omega\right)^{-1/2} \pm \left(1 + \frac{4\pi}{\mu_0}\frac{r^3\hbar}{g_1 g_2 \beta^2}\omega\right)^{-1/2}$$

† Historically, the transformation over τ was accepted in ESE spectroscopy, although the transformation over 2τ is more correct (in this case, the splitting in the doublet is ε_d).

(the 'plus' sign is used for thermally equilibrated pairs and the 'minus' sign is used for spin-correlated pairs). The frequency, ω, of two resonance lines varies from

$$\omega_{\perp} = \pm \frac{\mu_0}{4\pi} \frac{g_1 g_2 \beta^2}{r^3 \hbar}$$

to

$$\omega_{\parallel} = \mp 2 \frac{\mu_0}{4\pi} \frac{g_1 g_2 \beta^2}{r^3 \hbar}$$

[here, the signs have another meaning, namely, the upper (lower) sign is used for the first (second) term in Eqn (10)]. The first limit corresponds to $\theta = \pi/2$ (perpendicular orientation of RP). Here, a singularity appears in the spectrum. The second limit corresponds to $\theta = 0$ or $\theta = \pi$ (parallel orientation of RP) and determines the edges of the spectrum.

Almost always the spectrum is additionally broadened due to spin relaxation or distance distribution. A calculated spectrum for which the additional broadening was simulated by a Gaussian function with the half-width (between the points with maximum slopes) given by

$$0.05 \frac{\mu_0}{4\pi} \frac{g_1 g_2 \beta^2}{r^3 \hbar},$$

is shown in Fig. 3.

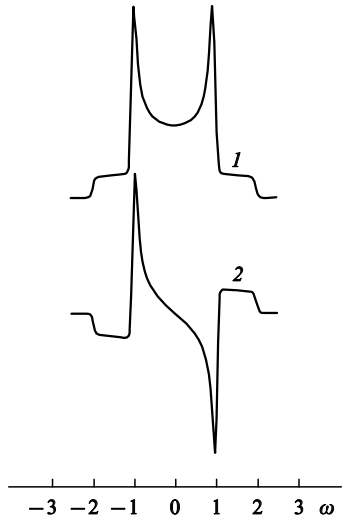


Figure 3. Dipolar doublet in polyoriented sample.
Thermally equilibrated radical pair (*1*) and spin-correlated radical pair (*2*). The frequency axis is labelled in

$$\frac{\mu_0}{4\pi} \frac{g_1 g_2 \beta^2}{r^3 \hbar}$$

units.

Often, only the singularity can be observed in the experimental spectrum because of relatively low intensities of other lines; knowing its position, it is possible to immediately determine the distance r.

The expressions for $\omega_{\perp}$ and $\omega_{\parallel}$ with allowance for the dipole–dipole and exchange (J) interactions in the pair take the form:[18]

$$\omega_{\perp} = \pm\left(\frac{\mu_0}{4\pi} \frac{g_1 g_2 \beta^2}{r^3 \hbar} - 2J\right), \tag{11}$$

$$\omega_{\parallel} = \pm\left(-2 \frac{\mu_0}{4\pi} \frac{g_1 g_2 \beta^2}{r^3 \hbar} - 2J\right).$$

Therefore, having established positions of the spectral singularity and the spectrum edges, one can determine the exchange interaction.

4. On the accuracy of the point dipole approximation

The point dipole approximation assumes that the whole spin density is localised at a certain point. Let us estimate the error introduced by the spin density distribution over the molecule. The measured parameter is ε_d, which is proportional to $1/r^3$ (r is the distance from a given spin to the partner spin). As the distance changes by Δr due to the spin density distribution, the variation, $\Delta\varepsilon_d$, is to a first approximation proportional to $-3\Delta r/r^4$. If the origin is at the 'centre of gravity' of the spin density (*i.e.*, the average value, $\langle \Delta r \rangle$, over the molecule is taken to be zero), the mean value $\langle \Delta\varepsilon_d \rangle$ in this approximation will also be zero. In the second approximation, $\langle \Delta\varepsilon_d \rangle$ is proportional to $6\langle \Delta r^2 \rangle / r^5$. As a result of this variation of ε_d, the distance measured in the point dipole approximation will have a systematic negative error

$$\delta r = -\frac{1}{3} \langle \Delta\varepsilon_d \rangle r^4 = -2 \frac{\langle \Delta r^2 \rangle}{r}.$$

Evaluation of the δr parameter for the radicals with an RMS spin density distribution width of $\langle \Delta r^2 \rangle = (1.5\,\text{Å})^2$ and a spin–spin separation of 30 Å using this expression gives a value of -0.15 Å. If the spin density distribution is known and can be taken into account in calculations of the dipole–dipole interaction, this small error can be made even smaller.

III. Experimental methods based on electron spin echo envelope modulation

If a MW pulse is applied to a spin system in the magnetic field at a frequency equal to the spin resonance frequency, the free induction signal is produced. The signal is maximum at a magnetisation flip angle of 90° and decreases with time owing to two reasons, (i) irreversible relaxation due to stochastic processes and (ii) phase defocusing due to static inhomogeneity of the resonance frequencies in the sample. Defocusing is reversible; application of a 180° pulse again produces the free induction signal at some delay after the second pulse. The delay time (τ) equals the time interval between two pulses. This signal is called the spin echo (Fig. 4 *a*).

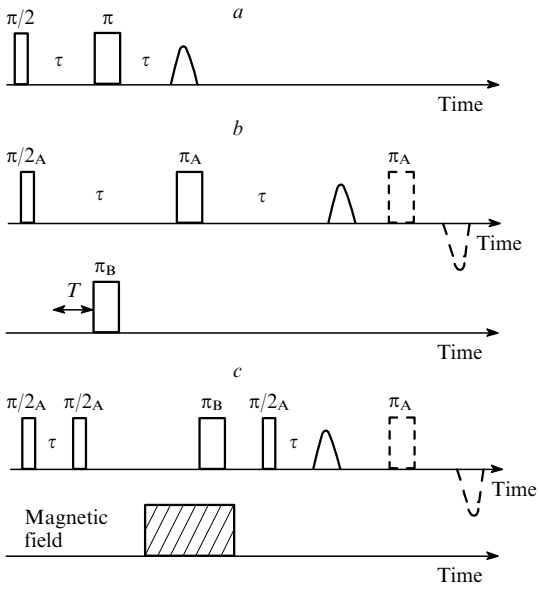


Figure 4. ESE pulse sequences used in studies of the dipole–dipole interaction between electron spins in radical pair.
Conventional two-pulse sequence (*a*), two-frequency double resonance (PELDOR) (*b*) and magnetic-field-jump PELDOR (*c*).

The origination of the echo signal is readily understandable from the following simple considerations. After application of the first pulse each spin precesses in its own local magnetic field as a result of static inhomogeneity of the resonance frequencies. Let us denote the deviation of the resonance frequency of a certain spin from the carrier frequency of the spectrometer as $\Delta\omega_0$. At the instant of application of the second pulse the phase change becomes equal to $\Delta\omega_0\tau$ (see Fig. 4 *a*). If $\Delta\omega_0\tau \gg 1$, the free induction signal decreases to zero because of averaging over all spins. Application of the second 180° pulse leads to phase reversal and the phase becomes equal to $\pi - \Delta\omega_0\tau$. Then, the phase changes again, namely, it changes with time as $\pi - \Delta\omega_0\tau + \Delta\omega_0(t-\tau)$, where t is the time passed from the first pulse. At $t = 2\tau$, all spins have the same phases equal to π and independent of $\Delta\omega_0$. This means the refocusing and the appearance of the echo signal.

The situation described above corresponds to a two-level spin system, for which the distribution over the energy difference between the levels ($\Delta\omega_0$ distribution) owing to various additional interactions is only possible. The situation becomes more complicated [as in the case of, *e.g.*, a radical pair (see Fig. 1)], if there are a number of energy levels and the MW pulses excite different transitions. This is accompanied by additional effects due to pulse-assisted alternation of magnetic interactions in the pair. In the text below we will show that such effects cause modulation of the echo signal decay on change in τ.

In this Section both spins in the pair are assumed to have rather long relaxation times ($> 10^{-6}$ s).

1. Modulation in two-pulse electron spin echo technique

The simplest experimental method suitable for studying the dipole–dipole interaction between spins in a pair is a conventional two-pulse echo technique. Application of the second pulse causes not only the precession phase reversal but also changes the orientation of the partner spin in the pair. As a result, the precession frequency is shifted by a value of ε_d and the spin-precession phase at $t = 2\tau$ is $\pi \pm \varepsilon_d\tau$ rather than π. The measured signal is proportional to $\cos\varepsilon_d\tau$, which means oscillation of the spin echo signal decay with τ. This phenomenon is termed an Electron Spin Echo Envelope Modulation (ESEEM).

Detailed calculations of ESEEM were carried out for spins in a thermally equilibrated pair [11] and for a more general case of arbitrary populations of the energy levels.[36] The effect of the flip angle of the first pulse was not considered in detail;[11] it was postulated to be the same as in the case of a single spin. In a more recent study [36] it was shown that this effect is more complex in character. However, the study [36] did not consider the effect of the flip angle of the second pulse, although earlier [11] mention was made of such an effect. Probably, both results obtained for arbitrary flip angles are inexact. For a conventional pulse sequence (90°–τ–180°–τ–echo) both calculations lead to the same results. The echo signal of a thermally equilibrated radical pair is given by

$$E(2\tau) = \sin^2 2\phi \cos\varepsilon_d\tau + \\ + \cos^2 2\phi \cos\left(\frac{1}{2}\sqrt{\varepsilon_d^2 + 4(\Delta\omega)^2}\,\tau\right)\cos\varepsilon_d\tau - \\ - \cos 2\phi \sin\left(\frac{1}{2}\sqrt{\varepsilon_d^2 + 4(\Delta\omega)^2}\,\tau\right)\sin\varepsilon_d\tau. \quad (12)$$

Note that the second and third terms on the right side of Eqn (12) at $\tau \neq 0$ are efficiently averaged owing to large inhomogeneous broadening ($\Delta\omega\tau \gg 1$). Only the first term is retained, which is proportional to $\cos\varepsilon_d\tau$. This is consistent with the simple qualitative consideration given above and, apparently, must be valid for all flip angles of the magnetisation vector. In the case of weak coupling ($\phi \approx \pi/4$) the role of the second and third terms is even less significant. In strongly coupled systems (this case is left out of consideration in this review) the signal is proportional to $\cos(3/2)\varepsilon_d\tau$, as mentioned above.

However, practical implementation of this two-pulse approach to studies of the dipole–dipole interaction in RPs faces some difficulties. First, MW pulses have a limited amplitude (usually, less than 1 mT) while the signal of, *e.g.*, nitroxyl biradicals has a total width of about 7 mT. Therefore, the probability of excitation of the partner spin in a pair (this is the necessary condition for applicability of this approach) is low. As a result, the effect of the signal decay modulation as compared to the large portion of non-modulated decays of single spins becomes weak. Second, not only the electron–electron but also the electron–nuclear interactions contribute to modulation. For nitroxyl biradicals, this contribution predominates.[22] Third, there is the 'dead' time problem, namely, the system's response cannot be measured immediately after the pulse is applied owing to transient processes in the cavity (usually, at $\tau < 100$ ns). It should be noted that reliability of the results of mathematical extrapolation to the 'dead' time region always casts some doubt.

There are a few studies on the observation of the modulation induced by electron–electron dipole–dipole interaction in two-pulse ESE spectra. Among them is a pioneering study [11] of RPs in single crystals containing no magnetic nuclei. A peak observed after Fourier transformation of the signal decay for nitroxyl biradicals dissolved in liquid crystals was attributed to the dipole–dipole interaction in the pair.[26] This peak was also recorded for polyoriented nitroxyl biradicals.[22] The contribution of this type of modulation was very small [22, 26] compared to the contribution of the electron–nuclear interaction.

Note that in the case of two-pulse ESE of photochemically generated spin-correlated RPs the difficulties mentioned above can be almost completely eliminated (see below).

The search for solutions to the problems posed in studies of radical pairs by the conventional two-pulse ESE method stimulated development of modified experimental techniques.

2. Pulsed electron–electron double resonance

PELDOR [12, 13] was the first modification of the ESE technique elaborated for the study of the ESEEM induced by the electron–electron dipole interaction. In this case the echo signal is excited using a conventional two-pulse sequence and an additional 180 pump pulse is applied at some other resonance frequency (see Fig. 4 *b*). The spins producing the echo signal are called A-spins and the partner spins in the pair (to which in this case the additional pulse is applied) are called B-spins.

The results of this experiment can be represented with ease using the phase ratios assuming weak spin–spin coupling. At time t, the phase of the A-spin after the first pulse is $[\Delta\omega_0 \pm (1/2)\varepsilon_d]t$ (the 'plus' or 'minus' sign depends on the projection of the B-spin). After the action of the 180° pulse applied at the B-spin frequency at time T the shift of the precession frequency due to the dipole–dipole interaction changes its sign and the phase at time τ (before application of the second pulse at the A-frequency) is given by

$$\varphi_A = \Delta\omega_0\tau \pm \frac{1}{2}\varepsilon_d T \mp \frac{1}{2}\varepsilon_d(\tau - T).$$

After the second pulse applied at the A-frequency one has

$$\varphi_A = \pi - \Delta\omega_0\tau \mp \frac{1}{2}\varepsilon_d T \pm \frac{1}{2}\varepsilon_d(\tau - T) + \Delta\omega_0(t-\tau) \mp \frac{1}{2}\varepsilon_d(t-\tau).$$

From here it follows that at $t = 2\tau$

$$\varphi_A = \pi \mp \varepsilon_d T.$$

The echo signal is proportional to $\cos\varepsilon_d T$, which means a modulation of the signal on change in time T at a frequency ε_d.

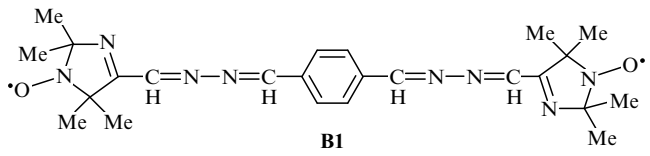
In the experiment, the pump pulse excites only a portion of the partner spins of a given A-spin. We will denote it P_B. Then, the probability of non-modulated signal decay is $(1-P_B)$ and the probability of modulated signal decay is P_B; the total signal is given by

$$V(T) = 1 - P_B + P_B \cos \varepsilon_d T. \quad (13)$$

The advantage of the PELDOR technique is the absence of electron–nuclear modulation. Indeed, application of a pulse at the B-spin resonance frequency does not change the electron–nuclear interactions of the A-spin. It is also important that in this case the 'dead' time problem is almost eliminated because the pulse at the B-frequency can be applied immediately after the first pulse at the A-frequency. The remaining uncertainty is due to the finite pulse duration. It can also be decreased by using an additional refocusing pulse at the A-spin frequency (see dashed lines in Fig. 4 *b*) and by positioning the pump pulse between the second pulse at the A-frequency and the additional pulse.[37] The position of the pump pulse can coincide with that of the echo signal excited by the first and second pulses at the A-frequency, which must correspond to zero time. Yet another advantage of the technique is that the signal modulation is not superimposed with the spin relaxation induced signal decay (as in the two-pulse method considered above).

At present, the PELDOR method is most widely used in studies of thermally nonequilibrated systems.

Except for the action on the B-spins at some other resonance frequency, the magnetic field can be changed in a stepwise fashion, as in the X- (see Ref. 38) and W-band EPR studies.[39] The pulse sequence is shown in Fig. 4 *c*. The A-spins were excited using the three-pulse stimulated echo sequence. The magnetic field jump synchronised with the 180° pump pulse was positioned between the second and third pulses. Due to the shift of the resonance field the 180° pump pulse affected only the B-spins. The three-pulse (instead of the two-pulse scheme, as in two-frequency PELDOR) scheme for excitation of the A-spins is used because the magnetic field jump in the two-pulse modification of the technique causes significant phase distortions for the A-spins. According to the three-pulse scheme, the magnetisation between the second and third pulses is retained along the Z axis of the rotating frame and the phase does not increase. The time τ between the first and the second pulses can be varied. Modulation is due to both the electron–electron and electron–nuclear interactions. The two mechanisms can be discriminated by switching the pump pulse off. Since both mechanisms are independent, their effect on the observed echo decay modulation must be multiplicative. This approach was employed in a magnetic-field-jump PELDOR study of rigid biradical **B1**.[38]



B1

The ESE signal decays of **B1** in protonated and deuterated solvents are shown in Fig. 5. The initial decays (see curves *1* and *2*) exhibit only the modulation at the frequencies of electron–nuclear interactions, while the result of division (curve *3*) is independent of the type of isotopes. Therefore, the observed ESEEM can be treated as electron–electron modulation. The results of Fourier transformation are shown in Fig. 6 (spectra *I* and *II*). Sharp lines seen in the spectrum correspond to singularities of the dipolar doublet (see Fig. 3 *a*). The distance between paramagnetic fragments — $r = 19.0 \pm 1.6$ Å was determined from positions of these singularities.

The dipolar doublets in spectra *I* and *II* exhibit no shoulders, which must appear according to theory (see Fig. 3). The absence of shoulders seems to be due to low intensities, which can be increased by orienting biradicals in the sample in such a manner that the line connecting both spins is parallel to the magnetic field direction. This can be done by placing the radical into a liquid crystal oriented in such a way that the axis of its director is parallel to the direction of the external magnetic field. The results of investigation of biradical **B1** are also shown in Fig. 6 (spectrum *III*).[38] As can be seen, the shoulders became much more intense. Exchange interaction was found to be zero from the shoulder positions using expressions (11).

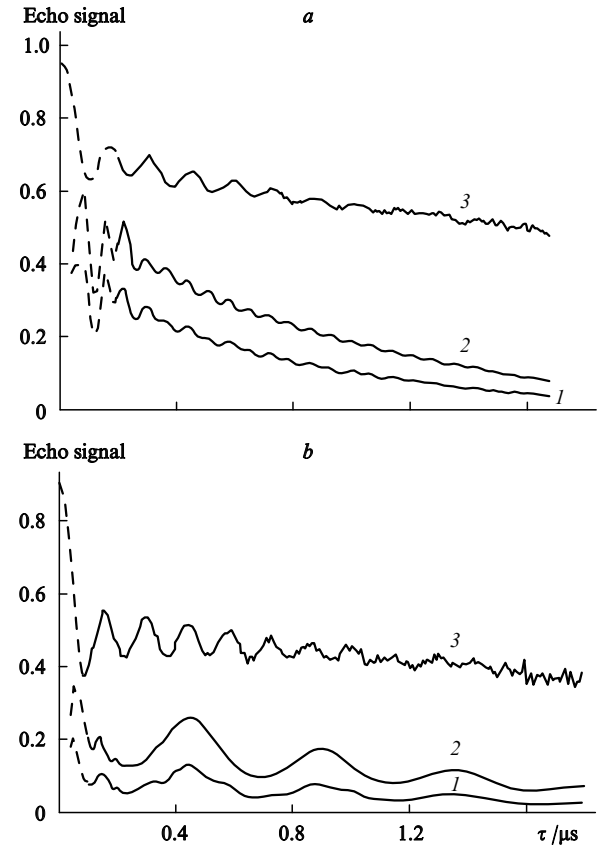


Figure 5. Magnetic-field-jump PELDOR signal decays obtained for biradical **B1** in toluene (*a*) and deuterated (*b*) toluene at 77 K.[38]
Signal decays obtained by τ scanning (see Fig. 4 *c*) (*1*); the same, but the pump pulse π_B is switched off (*2*); and curve *1* divided by curve *2* (*3*). The vertical axes are given in relative units for curves *1* and *2* and in absolute units for curves *3*. Dashed lines denote the results of signal recovery during the 'dead' time.

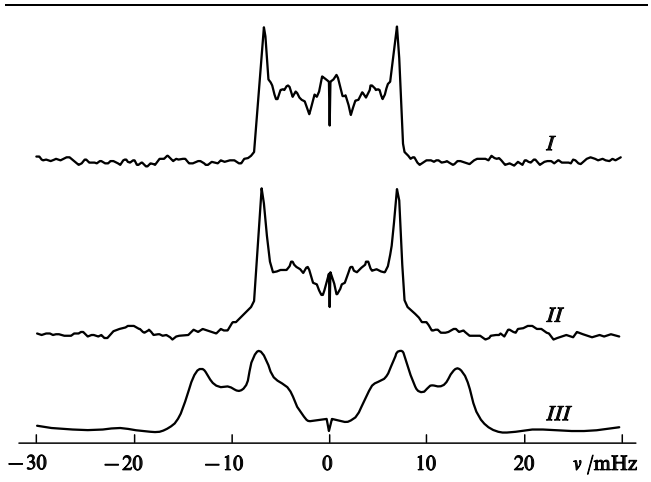


Figure 6. Results of cosine Fourier transformation of experimental data in the time domain.[38]
Experimental data: curve *3* in Fig. 5 *a* (*I*), curve *3* in Fig. 5 *b* (*II*); and data for biradical **B1** in oriented liquid crystal (the biradical axis is nearly parallel to the magnetic field direction) (*III*).

The advantage of the magnetic-field-jump PELDOR over the two-frequency PELDOR technique consists in the possibility of using a scanning pump [38] owing to an increase in the portion of spins (radical pairs) to be excited. Here, the 'dead' time can also be eliminated using an additional refocusing pulse. A drawback of the technique is the effect of relaxation processes on the echo decay.

A comparative PELDOR study of biradicals in two (X and S) EPR bands was carried out.[40] Since the electron – nuclear modulation depends on the MW band while the electron – electron modulation is independent of it, this approach can be employed to determine the contribution of electron – electron modulation.

The PELDOR technique cannot be used in studies of RPs with a relatively narrow EPR spectrum (less than 2 mT), where the excitation pump pulses and the reading pulses are superimposed and the effects observed are hard to interpret. Such spectra are typical of free radicals in photosynthetic reaction centres. It is more appropriate to study these systems by 'single-frequency' methods involving identical excitation of both A- and B-spins (see below).

3. The '2 + 1' method

The '2 + 1' method [14, 27] is much like the PELDOR technique considered above. It employs the same pulse sequences (see Fig. 4 *b*), but the pulses are applied at the one resonance frequency; *i.e.*, the basis pulse sequence is as follows: pulse 1 – T – pulse (+1) – ($\tau - T$) – pulse 2 – τ – echo. The echo signal appears after application of two pulses (pulse 1 and pulse 2); the additional pulse (pulse +1) is necessary to achieve alternation of the dipole – dipole interaction. Experiments involve variation of the time T at constant τ. The ESEEM occurs by the same mechanisms as in the PELDOR experiments; however, here both partner spins are excited identically.

In addition to the possibility of studying narrow spectra, the '2 + 1' method (compared to PELDOR) does not require an additional generator and special cavity. However, it also has significant drawbacks. First, the '2 + 1' technique is not free from electron – nuclear ESEEM. Elimination of this type of modulation requires special procedures, *e.g.*, comparison with a reference sample in which no dipole – dipole interaction occurs. Second, the dipole – dipole interaction alternates under the action of not only pulse +1 but also the second pulse (see above). Correct allowance for interference between these two effects is not always possible. For instance, if in polyoriented medium there are two types of pairs, with long and short distances, the major contribution to the echo signal will come from the pairs with the long distance, because the signal from the pairs with the short distance is rapidly damped due to alternation (see above). Therefore, in the presence of a distance distribution the distribution function will be significantly distorted. The PELDOR method is free from this drawback, because it usually involves observation at the edge of the spectrum, where only a small portion of A spins is excited.

4. Double-quantum coherence method

Using an appropriately designed pulse sequence, it is possible to excite a coherence between the highest and lowest levels in the scheme shown in Fig. 1.[15, 16, 26] A commonly used pulse sequence for this experiment (see Fig. 7 *a*) includes four pulses. Three of them ($\pi/2$ pulses) create a stimulated echo signal. The additional π-pulse is applied at the midpoint of the time interval between the second and third pulses.

The first two pulses create the double-quantum and zero-quantum coherences. They are refocused after applying the π-pulse and create a single-quantum coherence after application of the $\pi/2$ pulse observed as an echo signal. The contribution of the double-quantum coherence is selected using the pulse phase cycling from one series to another. Experiments involve variation of the time τ; the signal is modulated at the ε_d frequency.

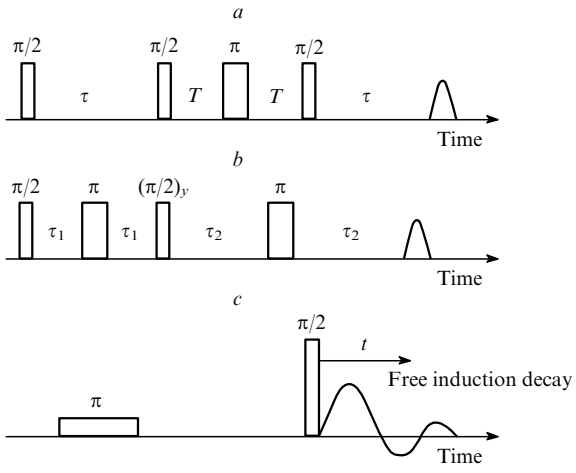


Figure 7. ESE pulse sequence used in studies of dipole – dipole interaction between electron spins in a radical pair.
Double-quantum coherence method (*a*), solid echo technique (*b*) and selective hole 'burning' (*c*).

In order to avoid the loss of signal during the 'dead' time, an additional refocusing (fifth) pulse or a six-pulse sequence is used, in which the double-quantum coherence is created by three ($\pi/2 - \tau/2 - \pi - \tau/2 - \pi/2$) rather than two pulses.[26] The advantage of the double-quantum coherence method is the absence of the interference effects described in the preceding chapter. However, in this case the electron – nuclear ESEEM occurs too. A drawback of the technique consists in a large number of phase change cycles (a total of sixty-four cycles), which can introduce an additional error. Besides, the phenomenon is characterised by a rather complicated theoretical description and the lack of a clear insight.

5. Solid-state NMR pulse sequences method

A Single-Frequency Technique for Refocusing (SIFTER) the dipole – dipole interactions was proposed.[17] It is based on the 'solid echo' and Jeener – Broekaert solid-state NMR pulse sequences. Consider the effects produced taking solid echo as an example.

The pulse sequence used in NMR is $(\pi/2)_x - \tau - (\pi/2)_y - \tau -$ echo. It permits refocusing of the dipole – dipole interaction between two nuclear spins (*e.g.*, protons in a bound water molecule in a crystal hydrate). The echo signal on the left and on the right of its maximum is modulated at the frequency of the dipole – dipole interaction. No 'dead' time problem is posed when observing this modulation. This gave an impetus to use of this pulse sequence in EPR as well.[17] However, this approach is only applicable to a pair of equivalent spins, when $\Delta\omega \ll \varepsilon_d$ (as in solid-state NMR). The reverse holds for EPR, which deals with inequivalent spins in the pair. This problem can be solved by adding two more refocusing $(\pi)_x$ pulses (see Fig. 7 *b*). At $\tau_2 = \tau_1$, the solid echo appears. This signal is created in such a fashion that static scatter of the resonance frequencies over the sample (except for their shift induced by the dipole – dipole interaction in the RP) has no effect on its shape. By varying the difference between two delays

$$t = \tau_2 - \tau_1$$

the observed signal can be modulated by the dipole – dipole interaction. This is performed at a constant total delay $\tau_2 + \tau_1$, which allows the relaxation effect to be excluded.

Selection of an informative signal is achieved by phase cycling (a total of three cycles). In order to suppress the electron – nuclear modulation of the decay, measurements are carried out at different total delays $\tau_2 + \tau_1$. Electron – nuclear ESEEM depends on this parameter, while the electron – electron ESEEM is independ-

ent of it. Therefore, averaging of the results obtained must lead to selection of the desired effect. For instance, the results of averaging over twenty-five values of this parameter were reported.[17]

This method is characterised by much simpler experimental design compared to the double-quantum coherence technique, because the number of phase change cycles decreases. However, theoretical description remains complicated and no clear representation of the phenomenon is available (the results can hardly be obtained without the density matrix formalism).

Thus, analysis of different methods of investigation of thermally equilibrated systems showed that PELDOR is the most convenient method. It provides a clear picture of the phenomenon and essentially simplified theoretical description. Besides, the electron – nuclear modulation effects are nearly completely eliminated. The only limitation of this approach is inapplicability to systems with narrow EPR spectra of RPs (biradicals).

6. Modulation of two-pulse out-of-phase electron spin echo for spin-correlated radical pairs

A chemical or photochemical reaction can produce spin-correlated radical pairs. An example is provided by photosynthesis in plants and bacteria. The process involves absorption of a light quantum followed by formation of a primary electron-donor radical cation and an electron, which is then consecutively trapped by different acceptor molecules to give corresponding radical anions. Initially, the pair is generated in the singlet spin state.

In this case only two inner energy levels are populated (see scheme in Fig. 1) . In accord with the portion of the singlet state [see Eqns (7)] the populations of four levels are as follows: $p_1 = 0$, $p_2 = \cos^2\phi$, $p_3 = \sin^2\phi$ and $p_4 = 0$. These populations are not thermally equilibrated; as a consequence, this gives rise to the spin polarisation effect. In weakly coupled systems this population distribution means that if one spin is in the α state, the second spin is in the β state, and *vice versa*. Therefore, such pairs are called spin-correlated pairs. In addition to the nonequilibrated populations, quantum-mechanical coherence of energy levels also occurs. However, these effects are rapidly damped (it takes less than 100 ns) and consideration of these phenomena goes beyond the scope of this review. The EPR spectrum of a spin-correlated radical pair exhibits two absorption and two emission lines (see Fig. 2 *b*), all line intensities being equal.

Calculations of the echo signals of spin-correlated states for a conventional two-pulse sequence (see Fig. 4 *a*) were carried out.[36, 41–43] We cite below the results [36] where coherence effects were averaged. Let us denote arbitrary initial populations as p_1, p_2, p_3 and p_4. Application of two pulses (θ_1 and 180°) along the X axis of the rotating frame creates an echo signal at $t = 2\tau$ with projections on the Y (in-phase echo) and X (out-of-phase echo) axes. The intensities of these signals are proportional to the corresponding magnetisations

$$M_x = P \sin 2\theta_1 [S_0 \sin^2 2\phi + \cos 2\phi (S_{-1} \cos^2\phi - S_{+1} \sin^2\phi)] +$$
$$+ \sin\theta_1 (p_2 - p_3) \sin^2 2\phi \cos 2\phi \left(S_0 - \frac{1}{2} S_{+1} - \frac{1}{2} S_{-1} \right), \qquad (14)$$
$$M_y = (p_4 - p_1) \sin\theta_1 \times$$
$$\times [C_0 \sin^2 2\phi + \cos 2\phi (C_{-1} \cos^2\phi - C_{+1} \sin^2\phi)],$$

where

$$P = -\frac{1}{2} p_1 + p_2 \sin^2\phi + p_3 \cos^2\phi - \frac{1}{2} p_4 ,$$
$$S_q = \sin\left(-\varepsilon_d \tau + q \frac{1}{2} \sqrt{\varepsilon_D^2 + 4(\Delta\omega)^2}\, \tau \right),$$
$$C_q = \cos\left(-\varepsilon_d \tau + q \frac{1}{2} \sqrt{\varepsilon_D^2 + 4(\Delta\omega)^2}\, \tau \right).$$

In thermodynamic equilibrium one has $p_2 = p_3$, $P = 0$ and the out-of-phase echo is absent; the expression for M_y coincides with Eqn (12). In contrast to this, only the out-of-phase echo is present for a spin-correlated radical pair born in the singlet state.

For inequivalent spins (weak coupling case), expressions (14) are significantly simplified:

$$M_x = -\frac{1}{2} (-p_1 + p_2 + p_3 - p_4) \sin 2\theta_1 \sin \varepsilon_d \tau, \qquad (15)$$
$$M_y = (p_4 - p_1) \sin\theta_1 \cos \varepsilon_d \tau.$$

An example of experimentally observed modulation is shown in Fig. 8 (an RP in Photosystem I). Figure 9 presents the results of Fourier transformation of these experimental data.

An amazing feature of the ESE in spin-polarised RPs is the absence of electron – nuclear modulation effects. First of all, this follows from good correspondence between the experimental and calculated spectra in the frequency domain (see Fig. 9 and curve *2* in Fig. 3); Fig. 9 exhibits no peaks that could be attributed to electron – nuclear interaction. A comparison of isotopically substituted samples ($^{14}N/^{15}N$, see Ref. 18 and $^1H/^2H$, see Ref. 44) led to identical results. Computer simulation [45] revealed that the absence of electron – nuclear modulation effects is due to polarisation of corresponding electron – nuclear transitions and mutual cancellation of corresponding peaks in the frequency spectrum of a polyoriented sample.

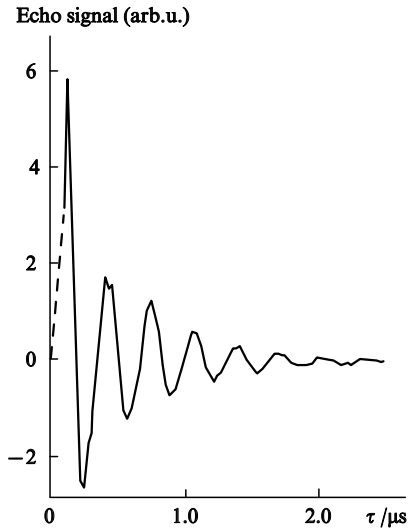


Figure 8. Out-of-phase echo signal modulation for $P_{700}^+A_1^-$ spin-correlated radical pair in Photosystem I.
Dashed line denotes the signal interpolated to the 'dead' time region.

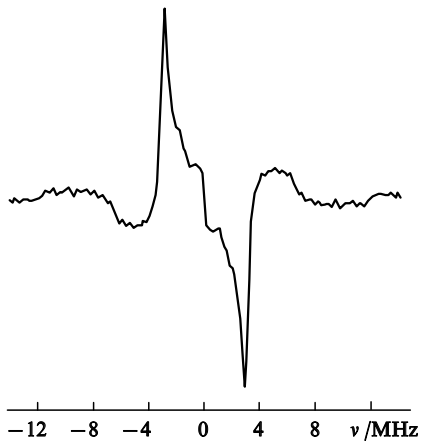


Figure 9. Results of sine Fourier transformation of the data shown in Fig. 8.

Yet another feature of the method is a sine-type dependence of the ESE signal amplitude on time τ. This allows the signal amplitude at $\tau = 0$ to be determined immediately (it with necessity equals zero). Thus, signal extrapolation to the 'dead' time region is reduced to a simpler case of interpolation (see Fig. 8).

Eventually, the linewidth in the spectrum of free radicals in photosynthetic reaction centres is of the order of 1 – 2 mT, which corresponds to the amplitudes of experimentally used MW pulses (excitation band). This means good conditions for excitation of both radicals in RP.

All these features of ESE experiments with spin-polarised RPs make the technique a rather efficient tool for investigation of structural features of the reaction centres.

7. Free induction decay modulation under selective excitation

This method employs the pulse sequence shown in Fig. 7 *c*.[46] The first small-amplitude 180° pulse selectively excites only one transition of a radical pair (see Figs 1 and 2). The action of this pulse is similar to 'burning' of a narrow hole in the spectrum. The second large-amplitude pulse excites all four transitions of the RP (non-selective pulse). It plays a dual role, *viz*., creates a free induction signal and changes the dipole – dipole interaction in the RP. Frequency interference between different transitions leads to modulation of the free induction decay at the frequency ε_d.[46] The technique provides a better signal-to-noise ratio for spin-correlated RPs compared to two-pulse ESE [46] and permits studies of zero-quantum and two-quantum relaxation times of RPs.

IV. Experimental methods based on spin relaxation

Methods employing the partner spin relaxation effects can be divided into two groups, namely, with fast and slow relaxation of B-spins. In the latter case both the A- and B-spins can be of the same type. The fast-relaxation case corresponds to the exchange narrowing of the splitting due to the dipole – dipole interaction, when $\varepsilon_d^2 T_{1B}^2 \ll 1$. Slow relaxation means that the reverse inequality holds. Rapidly relaxing spins are characteristic of metal ions. Slowly relaxing spins are typical of free radicals and also metal ions. Methods employed in the case of fast relaxation are based on the A-spin longitudinal (T_1-effects) and transverse (T_2-effects) relaxation rate measurements. In the case of slow relaxation, two methods are used, *viz*., selective hole 'burning' and dipolar modulation enhancement in stimulated ESE.

1. A-Spin longitudinal relaxation rate measurements. T_1-Effects

In the case of fast B-spin relaxation ($\varepsilon_d T_{1B} \ll 1$) the A-spin longitudinal relaxation rate (T_{1A}^{-1}) is related to the B-spin longitudinal (T_{1B}) and transverse (T_{2B}) relaxation times as follows:[47]

$$\frac{1}{T_{1A}} = \frac{1}{T_{1A}^0} + S_{rmB}(S_B + 1)\frac{\mu_0^2}{16\pi^2} \times \tag{16}$$
$$\times \left[\frac{b^2 T_{2B}}{1 + (\omega_B - \omega_A)^2 T_{2B}^2} + \frac{c^2 T_{1B}}{1 + \omega_A^2 T_{1B}^2} + \frac{e^2 T_{2B}}{1 + (\omega_B + \omega_A)^2 T_{2B}^2}\right],$$

where T_{1A}^0 is the time T_{1A} in the absence of B-spin, S_B is the B-spin and ω_A and ω_B are the A-spin and B-spin resonance frequencies, respectively

$$b^2 = \frac{1}{6} g_A^2 g_B^2 \beta^4 \frac{(1 - 3\cos^2\theta)^2}{\hbar^2 r^6},$$
$$c^2 = 3 g_A 2 g_B^2 \beta^4 \frac{\sin^2\theta \cos^2\theta}{\hbar^2 r^6},$$
$$e^2 = \frac{3}{2} g_A^2 g_B^2 \beta^4 \frac{\sin^4\theta}{\hbar^2 r^6}.$$

The T_{1A} time is measured in the signal recovery experiments after pulse saturation (or inversion). There are two types of experiments, (i) using an ESE spectrometer with pulsed signal detection (usually, by the spin echo technique) and (ii) using a pulsed EPR spectrometer with signal detection using a small-amplitude continuous-wave MW field. Various types of EPR spectrometers have been described.[48]

Determination of the distance r from expression (16) requires knowledge of the parameters T_{2B}, T_{1B}, ω_A and ω_B. Extended (in the frequency domain) spectra must be averaged over ω_A and ω_B. A severe problem consists in that not all B-spin transitions are observed experimentally. For instance, large zero-field splitting allows only one transition between the sublevels $m_S = \pm 1/2$ to be observed in the EPR X-band even for the Kramers ions, such as Fe^{3+}. Other non-observable transitions can also contribute to B-spin relaxation. Yet another important problem is complexity of the measurements with allowance for spectral diffusion, which is due to the excitation of a certain portion only of an inhomogeneously broadened EPR spectrum.

For these reasons, the results obtained using this approach are not always reliable and some of them were found to be erroneous. Therefore, in the present review the results obtained by this method are cited only in the case of some comparative experiments.

2. A-spin transverse relaxation rate measurements. T_2-Effects, relaxation probe method

If $T_{1B}|\omega_A - \omega_B| \gg 1$ (recall that $\varepsilon_d^2 T_{1B}^2 \ll 1$), the transverse relaxation rate is given by [47]

$$\frac{1}{T_{2A}} = \frac{1}{T_{2A}^0} + \frac{1}{2T_{1A}} + S_B(S_B + 1) \times \tag{17}$$
$$\times \frac{\mu_0^2}{16\pi^2} g_B^2 g_A^2 \beta^4 T_{1B} \frac{(1 - 3\cos^2\theta)^2}{3\hbar^2 r^6},$$

where T_{2A}^0 is the T_{2A} time in the absence of B-spin.

The transverse relaxation is measured from the ESE signal decay. This approach requires only knowledge of T_{1B}.

A measuring technique [49] involves determination of T_{1B} from the transverse relaxation of A-spins in the sample with uniform random spatial distribution of both types of spins. For such samples, the expression for the echo signal decay has the form [9]

$$v_{\text{random}}(2\tau) = \exp\left[-\frac{16\pi\sqrt{\pi}}{27}\sqrt{S_B(S_B + 1)} \times \right. \tag{18}$$
$$\left. \times \frac{\mu_0}{4\pi}\frac{g_B g_A \beta^2}{\hbar} C_B \sqrt{2\tau T_{1B}}\right].$$

where C_B is the concentration of B-spins.

From here T_{1B} can be found with ease. The technique has the advantage of self-consistency. In the case of pair and uniform spatial distribution, only one parameter (A-spin transverse relaxation rate) is to be measured and the same relaxation mechanism occurs. Here, the problem of inobservability of some B-spin transitions (see above) is by default completely eliminated. A limitation of the method consists in the necessity of preparing samples with uniformly distributed B-spins.

Often, radical and radical ion pairs produced in radiation-induced and photochemical reactions in solids are characterised by a large scatter of distances. The dependence of $(T_{2A})^{-1}$ on the separation in the RP [see Eqn (17)] allows one to set the problem of determination of the distance distribution function for RPs. This can be done by varying the temperature and thus the T_{1B} time, provided the physical properties of the sample do not change. The A-spins in the vicinity of B-spins do not contribute to the ESE signal. Thus, B-spins will be surrounded by a region of 'invisibility' for A-spins, the size of the region being varied with temperature. This approach can be called the relaxation probe method. Usually, the T_{1A} and T_{2A}^0 times depend on temperature much more weakly than T_{1B} (recall that usually the A-spins are the

organic radical spins and the B-spins are metal-ion spins). The distance distribution function for RPs can to a good accuracy be estimated by comparing the data of two experiments [49] as

$$n(r) = \frac{\mathrm{d}v_{\mathrm{pair}}(2\tau)}{\mathrm{d}[\ln(v_{\mathrm{random}}(2\tau))/C_{\mathrm{B}}]}, \tag{19}$$

where $v_{\mathrm{pair}}(2\tau)$ is the ESE decay for the sample with the pair distribution under study.

3. Selective hole 'burning'

Selective hole burning is used in the case of slow B-spin relaxation ($\varepsilon_{\mathrm{d}}^2 T_{1\mathrm{B}}^2 \gg 1$). Here, from Eqn (17) it follows that $T_{1\mathrm{B}} \gg T_{2\mathrm{A}}$, *i.e.*, the spin–lattice relaxation of B-spins is slow on the ESE time scale. Since the B-spins are usually the metal-ion spins with broad EPR spectra, in this chapter the possibility of their excitation by applying MW pulses will be ignored. This is the main difference of the technique in question from the selective excitation method considered above.

The pulse sequence employed in the selective hole 'burning' technique [21] is shown in Fig. 7 *c*. The first small-amplitude pulse 'burns' a narrow hole in the EPR spectrum, the hole width being of the same order of magnitude as the pulse amplitude. After time T the hole is broadened due to a change in the dipole–dipole interaction owing to spin–lattice relaxation induced fluctuations of the B-spin orientation.

Consider the A-spin whose resonance line is shifted by $\pm(1/2)\varepsilon_{\mathrm{d}}$ owing to the interaction with the B-spin (in our case the spin B is 1/2). After time T, the B-spin will change its value to the opposite with the probability $(1/2)[1-\exp(-T/T_{1\mathrm{B}})]$ and will retain it with the probability $(1/2)[1+\exp(-T/T_{1\mathrm{B}})]$. Thus, if initially the hole was described in the frequency domain by the function $h_0(\omega)$, after time T it will be given by

$$h_T(\omega) = \frac{1}{2}\left[1+\exp\left(-\frac{T}{T_{1\mathrm{B}}}\right)\right]h_0(\omega) + \\ + \frac{1}{2}\left[1-\exp\left(-\frac{T}{T_{1\mathrm{B}}}\right)\right]\left[\frac{1}{2}h_0(\omega-\varepsilon_{\mathrm{d}}) + \frac{1}{2}h_0(\omega+\varepsilon_{\mathrm{d}})\right].$$

Application of the second pulse causes the free induction decay (without changing the interactions in the system, because the excitation of B-spins is ignored), which corresponds to the Fourier image of the EPR spectrum. If we consider the difference between the signals in the presence and in the absence of the first selective pulse, the free induction decay can be described by the expression

$$H_T(t) = \int_{-\infty}^{\infty} \mathrm{d}\omega\left[1-h_T(\omega)\right]\cos\omega t = \tag{20}$$
$$= \frac{1}{2}\left[1+\exp\left(-\frac{T}{T_{1\mathrm{B}}}\right)\right] + \frac{1}{2}\left[1-\exp\left(-\frac{T}{T_{1\mathrm{B}}}\right)\right]\cos\varepsilon_{\mathrm{d}}t.$$

Thus, the free induction decay is modulated at the frequency ε_{d} and the larger the $T/T_{1\mathrm{B}}$ ratio, the larger the modulation depth.

Usually, substantial inhomogeneous broadening in EPR causes the free induction decay to be very short and to damp during the 'dead' time. But in the case in point the decay signal is observed due to the fact that it is created only by those spins whose resonance frequencies lie in a narrow spectral interval determined by the width of the hole.

4. Relaxation induced dipolar modulation enhancement and stimulated echo experiment

Consider a three-pulse sequence for stimulated ESE, $\pi/2-\tau-\pi/2-T-\pi/2-$echo. In the interval between the second and third pulses the B-spin changes its orientation with the probability $(1/2)[1-\exp(-T/T_{1\mathrm{B}})]$ and retains it with the probability $(1/2)[1+\exp(-T/T_{1\mathrm{B}})]$. Analysis of the spin precession phases between the first and second pulses, on the one hand, and after the third pulse on the other hand leads to the following expression for the echo signal decay

$$E(2\tau+T) = \frac{1}{2}\left[1+\exp\left(-\frac{T}{T_{1\mathrm{B}}}\right)\right] + \\ + \frac{1}{2}\left[1-\exp\left(-\frac{T}{T_{1\mathrm{B}}}\right)\right]\cos\varepsilon_{\mathrm{d}}\tau, \tag{21}$$

which means modulation at the ε_{d} frequency with scanning τ.[22] This permits determination of ε_{d}. The larger the T/T_1 ratio, the more pronounced the effect observed; therefore, this approach can be called Relaxation Induced Dipolar Modulation Enhancement (RIDME).

Expressions (20) and (21) are similar. This is not surprising because both methods, selective hole 'burning' and RIDME, are based on the same physical principle, being different in detection technique. Modulation is due to stochastic spin relaxation between pulses rather than the coherence effects upon excitation of different transitions in the spin system (see above).

There is an analogy with the PELDOR method, which involves an artificial change in the dipole–dipole interaction caused by application of the MW pulse. In the RIDME case the dipole–dipole interaction is changed by a natural process, spin-lattice relaxation. The advantage of the RIDME method is a much larger portion of the B-spins involved in modulation (P_{B}). From Eqns (20) and (21) it follows that this portion can be as high as 50%. (*cf.* P_{B} = 10%–20% for X-band PELDOR).

Due to inhomogeneous line broadening in high-field EPR the P_{B} parameter in the PELDOR becomes small and the modulation effect cannot be observed. For both relaxation methods described above (selective hole 'burning' and RIDME) this parameter is independent of the EPR frequency band. In particular, a high-field (4.5 T) RIDME EPR study was reported.[50]

A drawback of the relaxation methods is that other mechanisms, *e.g.*, intramolecular motions can also contribute to the relaxation observed.[51] Separation of these undesired contributions requires elaboration of additional experimental procedures. For instance, separation of the contributions of B-spin relaxation and methyl group rotation in a RIDME study [50] involved measurements of the temperature dependences of these contributions. The temperature behaviour of intramolecular motions obeys the Arrhenius relation while the T_1 time of free radicals is usually proportional to T^{-2}. In the latter case the temperature dependence is much weaker and by lowering temperature one can eliminate the contribution of intramolecular motions. A selective hole 'burning' study was reported, in which the contributions of other mechanisms were separated using a reference sample depleted of the particles bearing B-spins.[52]

5. Out-of-phase stimulated electron spin echo for triplet spin-correlated radical pairs

If a photoinduced spin-correlated pair comprises a radical and a short-lived triplet molecule, only the in-phase echo signal is initially observed.[53] Then, the out-of-phase stimulated echo signal appears, which proceeds in parallel with the decay of the triplet state. Variation of the time τ leads to modulation of both the in-phase and the out-of-phase echo signals at the frequency of the dipole–dipole interaction.

The modulation mechanism of the in-phase echo signal is similar to the RIDME mechanism (see above). The difference consists in that the RIDME modulation is due to a spontaneous shift of the spin resonance frequency caused by the spin-lattice relaxation induced change in the dipole–dipole interaction while in this case modulation is due to the change in the dipole–dipole interaction caused by the decay of the paramagnetic triplet state. The out-of-phase echo signal and its modulation are due to not only this reason but also the spin polarisation of the initial state of

the triplet – triplet RP. The in-phase and out-of-phase signals are described by the following equations:[53]

$$M_y = n_0 + (n_1 + n_{-1})\exp(-KT) + \quad (22)$$
$$+ (n_1 + n_{-1})[1 - \exp(-KT)]\cos\varepsilon_d\tau,$$
$$M_x = (n_1 - n_{-1})[1 - \exp(-KT)]\sin\varepsilon_d\tau,$$

where n_1, n_0 and n_{-1} are the initial populations of the corresponding triplet states of the RP and K is the decay constant of the triplet state.

Note that the out-of-phase signal appears only in the presence of the dipole – dipole interaction and only as a result of the decay of the triplet state. Besides, spin polarisation in the system is required.

Selective hole 'burning' experiments similar to those described above for spin-correlated RPs can be carried out with triplet RPs.[54] In this case the free induction decay signal becomes modulated.

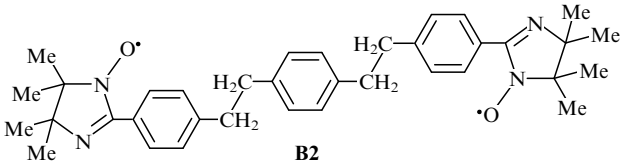
V. Conformations of long-chain biradicals and doubly spin-labelled and metal-containing biomolecules

1. Long-chain nitroxyl biradicals

Long-chain biradicals with single bonds in their structures can adopt a variety of conformations characterised by different biradical length. The distance between the terminal paramagnetic fragments can be used for characterisation of the conformational structure. The results of measurements of these distances in the shape-persistent biradicals, which are assumed to adopt only one conformation, are usually in good agreement with the results of structure simulations.[17, 22, 55, 56]

Flexible long-chain biradicals can adopt a larger number of conformations. In this case one must introduce a distance distribution function between paramagnetic fragments. Mathematically, this is an inverse problem of solving the Fredholm integral equation of the first kind. To this end, different methods were proposed, in particular, a truncated expansion of the kernel of the integral equation,[57] a discrete integral transformation of the equation with appropriately chosen transformation kernel (analogous to Fourier transformation) [33, 58] and the Tikhonov regularisation.[33]

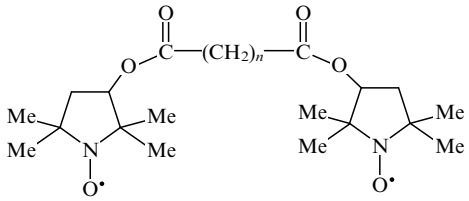
All these methods involve rather complicated computational procedures. If a narrow distance distribution is assumed, its width can be estimated immediately from the modulation decay.[38] This approach was employed in a magnetic-field-jump PELDOR study [38] of a shape-persistent biradical **B1** (see above) and a flexible radical **B2**.



B2

The ESE signal decays for **B1** are shown in Fig. 5 and the results of Fourier transformation are presented in Fig. 6. For the **B2** radical the modulation damped much faster than for **B1**. This can be associated with the presence of a distance distribution. The spin – spin separation estimated from the peak position in the frequency domain for **B2** was 20.5 Å. Damping of modulation for the shape-persistent biradical is due to scatter of the dipole frequencies caused by polyorientation of the sample. Any additional damping can be associated with the distance distribution. A comparison of the signal decays for **B2** and **B1** gave the distribution width $\Delta r = 3$ Å.[38]

Conformations of biradical



were studied by PELDOR.[58, 59] This biradical contains n methylene groups ($n = 8 - 20$). The average distances between the radical fragments were calculated from the frequency spectra obtained after the Fourier transformation of the decay traces. These data were compared with the results of calculations for the limiting case of completely stretched *trans*-conformation and with the results of the calculations of conformational statistics at the glass transition temperature of the polystyrene matrix. The results of distance measurements were found to be similar (within the limits of experimental error) to the calculated conformational statistics.

The distance distribution function for $n = 10$ was determined by the integral transformation and using the Tikhonov regularisation.[33, 58] Both methods gave similar results, namely, at $n = 10$, the width of the distribution function at half-height was ~ 5 Å at the average spin – spin separation $r = 21$ Å.

Determination of the distance distribution function in a sample with a complex mutual spatial distribution of RPs faces an additional problem of separation of the intrapair and pair – pair interactions. This is a complicated problem because of complex correlations between the radial and angular variables. However, angular spin – spin correlations of RPs can be neglected if the modulation depth of the echo signal decay is low.[58]

The PELDOR method is appropriate for measuring the dipole – dipole interaction not only in nitroxyl biradicals but also in biradicals containing paramagnetic metal ions as partner spins. As mentioned above, it is required that spin relaxation of the ion during the period of action of the pulse sequence be slow and the EPR spectrum be relatively narrow. A pulsed EPR study of a terpyridine-based Cu(II) complex containing phenylene- and ethynylene-based shape-persistent groups attached on two sides and two terminal nitroxyl labels was reported.[60] The observed decay modulation was interpreted as a result of dipole – dipole interactions in the copper – nitroxyl (distance 24.3 Å) and nitroxyl – nitroxyl (distance 48.6 Å) pairs.

The PELDOR method also allows the conformational structure of spin-labelled polymers (in essence, they are polyradicals) to be investigated. This can be done by monitoring the signal decay kinetics, which become non-exponential in the case of linear polymers (the cubic root of the time under the exponent). It is this decay law that was established in studies of spin-labelled poly(4-vinylpyridine) in a glassy solution.[61]

2. Doubly spin-labelled peptides and RNA

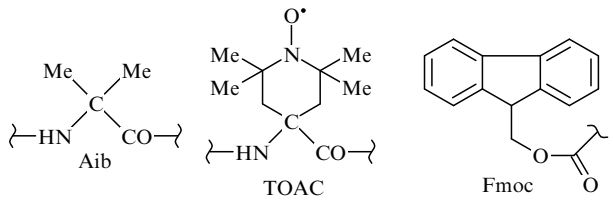
Recent development of biochemical methods of selective spin label attachment to specified fragments of biomolecules led to the wide use of this approach.[62, 63] The secondary structure of a doubly spin-labelled peptide can be established by studying the dipole – dipole interaction between the spin labels. If the distance between spin labels is shorter than 15 Å, continuous-wave EPR studies are carried out; for some results, see Ref. 64. If this distance exceeds 15 Å, the dipole – dipole interaction remains unresolved in continuous-wave EPR and one must use pulsed EPR spectroscopy.

A number of studies of doubly spin-labelled peptide trichogin GA IV have been reported.[65 – 70] This compound is a peptide antibiotic of fungal origin, rich in aminoisobutyric (Aib) acid, and possesses antibacterial and antifungal properties. Such peptides can produce ionic channels in membranes, which make them permeable and cause cell death.

A distinctive feature of trichogin GA IV is relatively small chain length. The length of the peptide is small compared to the membrane thickness; therefore, the mechanism of membrane permeability is still unclear. The peptide structure comprises three aminoisobutyric acid residues.

$$n\text{Oct}-\text{Aib}^1-\text{Gly}-\text{Leu}-\text{Aib}^4-\text{Gly}-\text{Gly}-\text{Leu}-\text{Aib}^8-\text{Gly}-\text{Ile}-\text{Lol}$$

In the chemical synthesis these residues are replaced by structurally similar nitroxyl spin labels TOAC.[68]



Two types of trichogin were used, namely, substituted trichogin (F-trichogin with n-octanoyl group replaced by Fmoc) and unsubstituted compound. Besides, the 1,2-aminoleucinol (Lol) residue was replaced by the L-leucine methyl ether (Leu – OMe) residue. These substitutions did not change the bioactivity of the peptides.[71]

Studies of doubly labelled (at positions 1 and 4, 4 and 8 and 1 and 8) peptides were performed. The first two types of biradicals were investigated by continuous-wave EPR[64] and the last type was studied by pulsed EPR spectroscopy owing to large spin – spin separation.

The conformation of spin-labelled F-trichogin-1,8

$$\text{Fmoc}-\text{TOAC}-\text{Gly}-\text{Leu}-\text{Aib}-\text{Gly}-\text{Gly}-\text{Leu}-\text{TOAC}-$$
$$-\text{Gly}-\text{Ile}-\text{Leu}-\text{OMe}$$

was studied by three-pulse PELDOR in various glassy solvents at 77 K. As a rule, no Fourier transformation was performed and the analysis was carried out in the time domain. The ESEEM observed in chloroform – DMSO solution was ascribed to the dipole – dipole interaction with the interspin separation of $\sim$20 Å.[65] The modulation damping was associated with the distance distribution of width $\sim$2 Å. It should be noted that only 25% of the labelled molecules are characterised by these parameters of the distribution function, while the remaining 75% of molecules are characterised by a broader distribution.

Doubly labelled trichogin-1,8 and F-trichogin-1,8 were also studied in other polar glassy solvents, *viz*., methanol, ethanol, trifluoroethanol and in chloroform/DMSO mixtures with different component ratios.[66] It was found that modulation significantly differs depending on the type of the molecule and the matrix. For F-trichogin-1,8, modulation is observed only in the chloroform/DMSO mixture, whereas for trichogin-1,8 it is observed in all matrices, but with different oscillation frequencies. The distances between paramagnetic fragments vary from 15.3 Å in trifluoroethanol to 21.8 Å in ethanol.

These distances can be compared with the structural parameters of peptides, established by X-ray scattering.[69,70] Using commonly accepted values for the peptide backbone torsion angles in the secondary structures (α-3_{10}-, 2_7- and 2_5-helices), one can calculate the interspin distances.[65,69,70] Based on the results of calculations, it was concluded that trichogin-1,8 and F-trichogin-1,8 adopt the 2_7-helix conformation in all matrices except for trifluoroethanol, where the peptides adopt the 3_{10} conformation.

The conformation of the same doubly labelled peptide in a tetrameric cluster formed in a matrix of low polarity (chloroform/toluene mixture) was studied.[67] The distance r = 15.7 Å is similar to the value 14 Å calculated for the 3_{10}-helix.

The structures of doubly spin-labelled proteins (lysozyme T4 mutants) were studied using the double-quantum coherence technique[72] in the 9 and 17 GHz bands. The distances found lie in the range from 20 Å (mutant 65/76) to 47 Å (mutant 61/135). High-quality spectra obtained made it possible to determine the distance distribution function. Analysis of this function revealed a variety of conformations of these molecules. The experimental results were compared with the results of molecular modelling.

The pioneering study[73] of spin-labelled RNA was carried out by the PELDOR method and involved two types of RNA with known molecular structures, labelled with nitroxyl labels in two positions of the uridine residue. According to structural data, the distance between paramagnetic fragments must be 35 Å for one type of RNA while the other type is characterised by a broad distance distribution. The results obtained coincided with the expectations, namely, the signal modulation observed in the former case corresponded to a distance of 35 ± 2 Å, whereas in the latter case no modulation was observed.

The PELDOR method was employed in determining the distance between two tyrosyl radicals in ribonucleic reductase *E. coli*.[74] The distance between two radicals found from the peak position in the frequency domain was 33.5 ± 0.4 Å. The modulation depth showed that at least 25% of radicals were in dimeric form (monomeric radicals can also be present in this system).

3. Metal-containing biomolecules

Many proteins and enzymes contain paramagnetic metal ions. If such ions form pairs and clusters, the mutual arrangement of these objects in space can be studied by EPR. In metal-containing biomolecules, the second spin can be delivered by incorporating a nitroxyl spin label. In some cases diamagnetic ions in proteins can be replaced by paramagnetic ions, *e.g*., Zn(II) by Co(II) and Mg(II) by Mn(II).

The spin relaxation of spin labels was studied over a wide temperature range in order to realise both fast and slow ion relaxation.[75–78] Transverse relaxation was studied by two-pulse sequence and longitudinal relaxation was studied by the saturation – recovery technique. Low-spin iron(III) porphyrins were investigated.[75] Raising the temperature from 8 to 120 K led to a decrease and then to an increase in T_2. Experimental data were analysed using the measured Fe(III) relaxation times. The distance in the metal – ion pair was estimated at 10.5 – 15 Å. High-spin iron(III)porphyrins were also studied.[76] Axial ligands were fluorine, chlorine and bromine. The temperature dependence of T_2 exhibited a minimum near 6 K. The experimental data were analysed using independently determined iron relaxation rates. The interspin distances were between 11.6 and 15.0 Å, which is in agreement with the values obtained for low-spin iron (see above). A study[77] of low-spin methemoglobins spin-labelled at the cysteine β-93 position revealed a decrease and then an increase in T_2 value with an increase in temperature from 6 to 120 K. The distance in the spin label – ion pair (15 – 15.5 Å) was determined analogously. These distances in high-spin fluoro- and aquamethemoglobins increased to 15.8 – 17.5 Å.[78]

The PELDOR method was employed to study the dipole – dipole interaction between two paramagnetic centres (PCs) in [3Fe – 4S](+) and [NiF] clusters in *Desulfovibrio vulgaris Miazaki F*. hydrogenase.[79] The distance between PCs, known from X-ray data, differs from the PELDOR measured value. Probably this is due to specific exchange binding in the iron/sulfur cluster. Nevertheless, such studies make it possible to collect information on the internal structure of multinuclear metal clusters.

The Mo(V)/Fe(III) state of sulfite oxidase was studied by the PELDOR method in different (X- and C-) MW bands at 4.2 K.[80] A-Spins were the Fe(III) ion spins. Analysis of the decay curves suggested multiple conformations of the flexible loop connecting the Mo and Fe.

VI. Cluster nanostructures

1. Peptide clustering in non-polar media

Peptides can form clusters or aggregates; this property can play the determining role for their physiological functions. ESE

spectroscopy provides a unique possibility of studying the clustering of spin-labelled peptides. All known experimental techniques employed in such studies are based on the same principle. We will consider it taking the PELDOR method as an example.

The echo signal from radicals in an RP is given by expression (13). Assume that a cluster comprises N particles and that the probability of simultaneous excitation of more than one B-spin is low, *i.e.*, $P_B N \ll 1$. Then, for the nth particle ($n = 1, 2, ..., N$) one has

$$V_n(T) = \prod_{k \neq n} \left[1 - P_B + P_B \cos\left(\varepsilon_d^{nk} T\right)\right],$$

where ε_d^{nk} is the parameter of the dipole–dipole interaction with the kth spin.

This expression should be averaged over all possible pairs. At low P_B, the averaging can be performed independently for each pair

$$V(T) = \left[1 - P_B \langle 1 - \cos(\varepsilon_d T)\rangle\right]^{N-1}.$$

From this it follows that at $t \to \infty$ the quantity $V(T)$ tends to the limit

$$(1-P_B)^{N-1} \approx 1-(N-1)\, P_B\,. \qquad (23)$$

The number, N, of particles in the cluster can be estimated from the asymptotic (long-time) ESE kinetics.

This approach was used in PELDOR and continuous-wave EPR studies of the aggregation of spin-labelled peptide trichogin GA IV (see Section V) in glassy polar and low-polar solutions at 77 K.[81] It was hypothesised that the peptide forms channels in membranes by forming a bundle comprising a number of molecules with polar groups directed to the interior and hydrophobic groups pointing to the exterior. However, numerous previous studies revealed no aggregation. Two types of solvents were a chloroform/toluene (7 : 3) and a chloroform/toluene/ethanol (3.5 : 1.5 : 5) mixture. The choice of the mixture compositions was determined by two factors, the peptide solubility and the formation of glassy state on freezing. The first mixture was a medium of low polarity while the second mixture was a polar liquid. Peptides were spin labelled at positions 1 and 4.

Continuous-wave EPR studies of various media at 77 K revealed the absence of spectral differences. The PELDOR data are shown in Fig. 10. A smooth signal decay observed in the polar matrix is characteristic of uniform intermolecular distribution. In the non-polar matrix, a dramatic signal decay occurs at times 100–150 ns, which is much more pronounced than that of F-trichogin-1,8 biradical shown for comparison.

This behaviour can be explained by aggregation of molecules in the non-polar matrix. Using expression (23) and the data for a model biradical system, one can immediately estimate the number of molecules in the aggregate. Indeed, in both cases the portion, P_B, of excited spins (in this case, $N = 2$) can be found from the asymptotic data for the biradical given identical experimental conditions with allowance for similar EPR spectral pattern. Knowing P_B from the asymptotic data (see Fig. 10), one can immediately determine $N \approx 4$ in the solution of low polarity. Thus, this peptide forms tetrameric clusters in the glassy solution of low polarity.

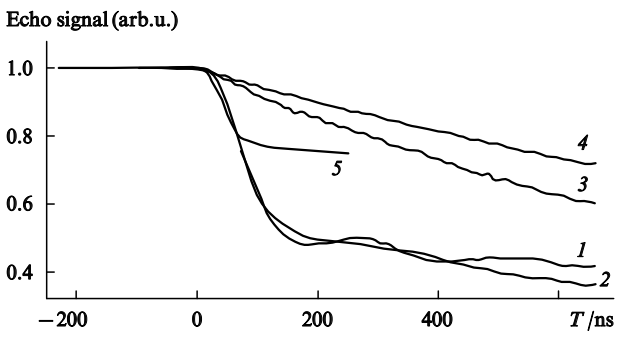


Figure 10. Two-frequency PELDOR signal decays obtained for peptide glassy solutions with scanning time T (see Fig. 4 *b*) at 77 K.[81]
F-trichogin-4 (*1*) and trichogin-4 (*2*) in chloroform/toluene mixture; F-trichogin-4 (*3*) and trichogin-4 (*4*) in chloroform/toluene/ethanol mixture and doubly labelled peptide F-trichogin-1,8 in methanol (*5*).

The signal modulation observed in the experiments (see Fig. 10, curves *1* and *2*) can be explained by narrow distribution of the distances between spin labels in the cluster structure. The cluster size estimated from the initial decay rate (at times shorter than 150 ns) is 30–36 Å. The distances determined from the decay modulation for F-trichogin-4 and trichogin-4 are 23.5 and 26.0 Å, respectively.[81]

It is noteworthy that these solvents exhibit significantly different room-temperature continuous-wave EPR spectra.[81] The EPR lines in the spectrum of the solvent of low polarity are much broader; this is similar to line broadening due to slowing down of the orientation motion, which is known in the EPR of spin labels and probes. This should be expected in the case of clustering, because the orientation relaxation time is proportional to the particle size according to the Stokes–Einstein–Debye relation. The cluster size was estimated from the broadening of the continuous-wave EPR spectra.[82] The results of measurements coincided with the estimate of the number of molecules in the cluster ($N \approx 4$). Therefore, the results obtained by both continuous-wave EPR of liquids at room temperature and by PELDOR of glassy frozen solutions substantiate the peptide clustering.

Analogous measurements were carried out for mixtures of other solvents of low polarity, namely, chloroform/toluene, carbon tetrachloride/toluene and dichloroethane/toluene.[83] In all cases, aggregation was revealed, with $N \approx 3.1$–4.3 depending on the system. The modulation observed corresponded to inter-spin distances of 23, 26 and 33 Å, respectively (one distance or a set of distances depending on the system).

Aggregation of spin-labelled zervamicin IIA (a hexadecapeptide of fungal origin) was investigated.[84] This compound is known to form hollow channels in phospholipid double layers. The PELDOR study of frozen glassy mixtures in the toluene/methanol system at 77 K revealed aggregation. The average distance between spin labels was 25–35 Å (depending on the mixture composition). It was concluded that peptide molecules have an antiparallel orientation and that the increase in the methanol concentration in the mixture led to loosening in the cluster structure.

No aggregation of spin-labelled trichogin dimers (covalent compounds comprising two molecules linked 'head-to-tail') in methanol was observed, but it did occur in a chloroform/toluene mixture (2 to 3 molecules).[85] The distances between spin labels in clusters were found to be in the range from 30 to 45 Å. An increase in the peptide concentration in non-polar solvents led to formation of tetrameric clusters.[86]

A double-quantum coherence ESE study [16] revealed clustering of peptides MTSL–CPPPPC–MTSL in a glycerol/water/trifluoroethanol mixture at −82 °C. An increase in the peptide concentration from 0.75 to 3 mmol g^{-1} was followed by the appearance of the double-quantum coherence signals from both intramolecular and intermolecular pairs. In the latter case the parameters of the signal indicated a high local spin concentration. Clustering was observed in a polar matrix. A structurally similar peptide MTSL–CPPPC–MTSL showed no aggregation.[16]

2. Nanostructure of ionomers

Ionomers are polymers with terminal ion groups.[87,88] Their structures contain clusters of ion groups of the size of a few nanometres separated by distances of the same order. Both these parameters of the nanostructure can be evaluated using ionic spin probes.[33,89,90] A study of ionomers based on a polyisoprene/polystyrene copolymer showed that ion groups can cap one or

both chain ends or be situated at the polyisoprene/polystyrene interface. It was shown that the surface of ion clusters is accessible to ionic probes.[91]

Experiments [33, 89, 90] were carried out using the PELDOR method. The concentration of spin probes was chosen to provide on the average two probes per cluster. The temporal evolution of the PELDOR signal was treated as a result of manifestation of the pair distribution function represented by a superposition of two Gaussian curves and a uniform distribution. The Gaussian curves corresponded to the distances $r_1 \approx 2$ nm and $r_2 \approx 5-7$ nm, where r_1 is the characteristic interparticle distance in the cluster and r_2 is the characteristic intercluster distance.

A comparative experiment with a non-polar spin probe revealed only a uniform distribution. The results obtained for three ionic spin probes characterised by increasing distance between the nitroxyl and ionic groups substantiated the interpretation mentioned above. A shift of the first distribution peak towards longer distances [89] was interpreted as additional evidence for the fact that the probe is situated on the surface (with the nitroxyl group directed inside the polymer chains) and that this peak should be attributed to the cluster size. SAXS data [91] are consistent with the PELDOR data [33] given some assumptions concerned with specific features of the interpretation of the results obtained by both methods.

Studies of polymers with different molecular masses and, hence, different chain lengths revealed that the cluster size is independent of the molecular mass except for the cases where the size of the ionic group is much shorter than the chain length. The cluster–cluster distance must be a linear function of the chain length. Such a correlation established for polymers with ionic caps at one end [33] has the form

$$r_2 \sim M^{0.334},$$

where M is the molecular mass of the cluster. Polymers ion-capped at both chain ends (an anion at one end and a cation at the other end of the polyisoprene/polystyrene copolymer) exhibited no correlation between r_2 and M. This is due to specific features of the polymer packing, which is characterised by the formation of the polyisoprene/polystyrene interface containing surface ionic groups. In this case an increase in M can have no effect on the mutual arrangement of clusters on the surface.

VII. Stable paramagnetic pairs in photosynthetic reaction centres of plants and bacteria

1. Radicals and ions in photosynthetic reaction centres

Photosynthesis in higher plants, algae and some bacteria occurs in the photosynthetic reaction centres. These are protein complexes containing a number of cofactors that absorb the energy of a light quantum and participate in subsequent charge separation, producing radical pairs comprised of paramagnetic radical cations and radical anions. Besides, the RC structure *a priori* contains paramagnetic ions. Therefore, EPR spectroscopy can be an efficient tool of research on the structure and operation of RC.[92–95]

The RC structure was the subject of a number of X-ray studies (see, *e.g.*, Refs 96–102 and references cited therein). These methods require crystallisation of samples. The spatial resolution varies from 2 to 4 Å depending on the complexity of the system and the quality of the crystals. Molecular modelling [103] is also a useful tool in structure analysis; here, conclusions about the structure of more complex systems are drawn based on the known data of relatively simple systems (purple bacteria RC).

Pulsed EPR studies of RC offer the following advantages. First, preparation and modification of samples (by *e.g.*, artificial replacement of cofactors) are much less labour-consuming processes compared to their crystallisation (corresponding artifacts are also ruled out). Second, higher spatial resolution permits refinement of the supramolecular structure established by other methods and in some cases facilitates the interpretation of data. Third, the observation of photo- and thermally induced structural rearrangements becomes possible. Finally, it is possible to investigate the interrelations between the structure and the functioning of the RC, because EPR studies are directly related to the cofactors responsible for electron transfer.

The bacterial RC has the simplest structure. Corresponding data were obtained with the highest resolution, 2.3–3 Å.[96–99] The RC contains a primary electron donor, namely, a bacteriochlorophyll dimer, which is usually denoted as P_{870} (the subscript denotes the maximum wavelength of the optical absorption band, expressed in nanometres). Absorption of a light quantum produces a radical cation P_{870}^+ and an electron, which migrates along the chain of other cofactors. The migrating electron consecutively forms corresponding radical anions. First, it arrives at the bacteriochlorophyll molecule adjacent to the dimer, then at the bacteriopheophytine molecule, at the primary quinone acceptor, Q_A, and at the secondary quinone acceptor, Q_B. Each charge separation step involves two particles (a radical pair). The dimer cation is reduced owing to electron transfer from the nearest cytochrome molecule. After absorption of two light quanta the doubly reduced Q_B is protonated to quinone and leaves the reaction centre. Its position is then occupied by another quinone from the so-called quinone pool, and the process can proceed again. The bacterial RC also contains a paramagnetic non-heme Fe(II) ion. All cofactors have their 'twins' arranged symmetrically with respect to the line connecting the centre of P_{870} and the iron ion (symmetry group C_2, the P_{870} dimer also has a symmetrical structure). Thus, there are two pathways, A and B, the charge separation process following only the former. The reason why pathway B is not involved is still unclear.

Photosynthesis in higher plants is a much more complicated process and involves consecutive operation of two RC, photosystem II (PS II) and photosystem I (PS I). It is known that operation of these RCs results, in particular, in the evolution of oxygen from water molecules. This occurs in the so-called oxygen-evolving complex (tetranuclear manganese cluster).

The structure of PS I was established by X-ray analysis with a 4 Å resolution.[100] In PS I, an electron is initially transferred from the primary chlorophyll donor P_{700} to the chlorophyll molecule (A_0) and then to the phylloquinone molecule (A_1). This results in a $P_{700}^+A_1^-$ pair.

The structure of PS II was also established by X-ray analysis with a 3.7–3.8 Å resolution.[101, 102] The protein backbone of PS II contains a number of cofactors analogous to the bacterial RC, *i.e.*, the chlorophyll electron donor P_{680}, pheophytine, plastoquinone and non-heme iron(II). It is believed that these cofactors also form a structure with a C_2 symmetry, which is similar to the bacterial RC. Plastoquinone Q_B is transformed into plastoquinol, which becomes an electron donor for PS I *via* cytochrome b_6f; P_{680}^+ is reduced by tyrosine Y_Z. There is yet another symmetrically arranged tyrosine molecule Y_D whose function is unclear as yet.

The oxidation of the manganese cluster occurs in a stepwise manner on consecutive absorption of light quanta. As a result, absorption of four light quanta leads to splitting of two water molecules into four protons and four electrons *via* five intermediate states, namely, S_0, S_1, S_2, S_3, S_4 (transition from the S_4 state to the S_0 state is a dark transition) and eventually gives an oxygen molecule.[104] A number of models for the operation of this cluster are available (see, *e.g.*, Ref. 105).

Under laboratory conditions, different states of the S_0-S_4 cycle can be achieved by specific biochemical treatment, irradiation and freezing. A broad multicomponent EPR signal of tetranuclear manganese cluster with spin 1/2 is observed in the S_2 state.

2. Stable paramagnetic pairs

$P_{870}^+-Q_A^-Fe^{2+}$ pairs in the RC of purple bacteria *Rhodobacter sphaeroides* R26 were studied [106] using the selective hole 'burning' technique. A distance of 26 ± 2 Å determined in the experiments is in good agreement with the data of X-ray analysis. This was

treated as a substantiation of correctness of the method employed; later, this technique was used in studies of other systems.

The $Y_Z - Mn_4$ pair in PS II was investigated by saturation–recovery ESE [107] and a 15 Å distance was determined. Possible sources of errors in the technique were reported in another study.[108] It should be noted that the dipole–dipole interaction in this pair is well observed by continuous-wave EPR; analysis of the lineshape by different authors gave a distance of ~ 8 Å.[109–112]

Measurements for the $Y_D - Mn_4$ pair in PS II were carried out by different ESE spectroscopy methods, in particular, the selective hole 'burning' technique.[52] In this approach, it is of crucial importance to exclude all sources of hole broadening except for those associated with the dipole–dipole interaction. This was achieved by comparing the spectra obtained with the spectra of a sample containing no manganese complex. To attain a better agreement with the experiments, it was assumed that the manganese complex is characterised by non-exponential spin-lattice relaxation with a small contribution (12%) of a 'long-tail' component. In addition, a distance distribution in the range 4–6 Å was assumed. Measurements for the S_2 state gave a distance of 28 Å. A similar value of 27 ± 0.2 Å was obtained by the PELDOR method.[113]

The results of these investigations revealed an essentially unsymmetrical arrangement of Y_D and Y_Z with respect to the manganese complex. A rather long distance from the complex to Y_D suggests that the latter is not involved in primary electron transfer.

The dipole–dipole interaction in the Y_D and Y_Z pairs in PS II was studied by the '2 + 1' method[114] using samples depleted of manganese complex. A distance of ~ 30 Å was determined. This approach was employed also to study oriented membranes.[115] The angle between the radius vector of the pair and the normal to the membrane surface was found to be $100 \pm 2^\circ$.

Oriented membranes depleted of manganese complex were studied by the '2 + 1' technique.[116] The angle between the vector connecting Y_D and Chl_Z and the normal to the membrane was found to be $50 \pm 5^\circ$. The separation in the pair, obtained for a polyoriented sample, was 29.4 ± 0.5 Å.[116,117] The distance in the $Y_D - Q_A^-$ radical pair studied by the same method was 38.8 ± 1.1 Å.[117]

The Y_D–Fe(II) pairs in PS II were investigated by the selective hole 'burning' technique.[106] The distance was 42 ± 2 Å. Calculations carried out with allowance for zero-field splitting gave a value of 0.81 for the effective spin of the ion.

Data for the Y_Z–Fe(II) and Y_D–Fe(II) pairs were obtained using the saturation–recovery method.[118] As mentioned above, the technique is inappropriate for obtaining reliable quantitative data, but qualitative information can appear to be useful. Samples depleted of manganese complex were studied. In the mutants containing no Y_D it is possible to characterise the Y_Z–Fe(II) pair. It was found that Y_Z and Y_D obey identical saturation–recovery kinetics. This suggests that both tyrosines are at equal distances from Fe(II), being arranged symmetrically with respect to Fe(II).

VIII. Photoinduced spin-correlated pairs in photosynthetic reaction centres of plants and bacteria

Isolated RC make it possible to investigate short-lived RPs produced after absorption of a light quantum in the course of electron transfer. For instance, no electron transfer beyond Q_A occurs in bacterial RC at low temperatures; the $P_{870}^+Q_A^-$ pair has a lifetime of 30 ms and disappears *via* reverse recombination. The distance in the pair (~ 25 Å) makes it a convenient subject for ESE spectroscopy studies. Since the pair was born in the singlet spin state, the spins are not thermally equilibrated and we deal with a spin-correlated pair. Therefore, the use of ESE spectroscopy is of additional interest for studying spin correlation effects.

The ESE signal of a radical pair in photosynthetic RC was first detected by Thurnauer and Norris.[119] It was found that the signal phase is shifted by 90° compared to the signals of thermally equilibrated systems (the out-of-phase signal). The nature of the signal and of the phase shift remained unclear at that time. The theory of ESE in spin-correlated radical pairs was developed much later [41,42] and it does predict the out-of-phase signal for spin-correlated RPs (see Section III).

This theory also predicts that an increase in the interval between pulses will cause modulation of the two-pulse ESE signal (ESEEM) at the frequency of the dipole–dipole interaction in the pair. However, first experimentally observed ESEEM [120] was attributed to the electron–nuclear interaction and not analysed. A long time after it was established that the electron–nuclear interaction in spin-correlated RPs does not manifest itself and the observed modulation is completely governed by the electron–electron interaction in the pair.[18,44] This was substantiated not only by good agreement between the experimental and theoretical dipolar doublet but also by the results of the $^{14}N/^{15}N$ and H/D isotope substitution experiments.[18,44]

The reason for the absence of the electron–nuclear contribution in ESEEM (which strongly complicates measurements of the dipole–dipole interaction in thermally equilibrated pairs) seems to be polarisation of electron–nuclear transitions, whose lines are mutually cancelled in the frequency domain of a polyoriented sample.[45]

Numerous studies of RPs in photosynthetic RC by the out-of-phase ESE decay modulation have been carried out since publication.[18] Because of the absence of an electron–nuclear contribution, correspondence between the width of the EPR spectrum and the excitation bandwidth of an ESE spectrometer and ease of signal interpolation to the 'dead' time (see Section IV) the dipolar doublet appears to be similar to the theoretical one (see Figs 3 and 9). Not only the perpendicular but also the parallel orientation is well resolved. This permits determination of the distance in the pair with a very high accuracy (up to a few fractions of an Ångström) and analysis of subtle effects due to structural changes under the action of external factors.

Three types of RC, namely, bacterial, PS I and PS II ones are characterised by production of structurally similar RPs in the initial steps of electron transfer. Pairs comprised of a primary electron donor and a primary quinone acceptor are convenient for ESE studies.

1. Bacterial reaction centres

At low temperatures, no electron transfer from Q_A to Q_B occurs in the reaction centres of purple bacteria *Rhodobacter sphaeroides* R26, and a radical pair $P_{870}^+Q_A^-$ with a lifetime of 30 ms is produced; then, it disappears *via* reverse recombination. This pair was studied in Zn-substituted samples.[18,44,121,122] The out-of-phase echo signal was detected, which was strongly modulated with τ. The distances in the pair were determined by analysing the dipolar doublet in the frequency domain. The structures of these RC were established by X-ray diffraction; therefore, one of the goals was to evaluate the new experimental technique.

It was found that the distances in the pair, obtained in different studies, are also different. According to X-ray scattering data, the distance in the pair must be 28.1 (see Ref. 98) or 29.2 Å,[99] but the dipole–dipole interaction in the pair corresponded to a shorter distance.[18] The distance in freshly prepared samples was 28.9 Å,[122] being in good agreement with the X-ray structural data. These discrepancies were attributed to 'ageing' of the sample, *i.e.*, a change in its structure in the course of long-term storage (the authors of study [18] used the samples kept at a liquid nitrogen temperature for months). The distance 28.4 Å [44,121] is similar, within the limits of error, to the results obtained in Ref. 122.

Good correspondence with the X-ray structural data suggests that the method based on the out-of-phase echo signal decay modulation provides correct information on the distances in the

pair. It should be noted that these methods are used to study different systems. X-Ray analysis deals with a crystalline sample, does not involve exposure to light and no charges are produced in the system. ESE investigations are usually carried out with amorphous samples (although it can also be crystalline, see below), being aimed at studying a pair comprising two oppositely charged particles. Therefore, the results obtained also mean that these differences cause no pronounced structural changes. In particular, the electrostriction effects in the course of charge separation must be insignificant.

A study of the RC of *Rhodopseudomonas viridis* bacteria in Zn-substituted samples treated with *o*-phenanthroline in order to block electron transfer to Q_B was reported.[123] The distance in the $P^+_{960}Q^-_A$ pair also appeared to be similar to that determined by X-ray scattering.[124]

The temperature dependence of the shape of the dipolar doublets found for the bacterial RC at cryogenic temperatures [122] was interpreted as a result of rearrangement of the RC protein backbone on changes in the temperature.

2. Reaction centre of PS I

Spin-correlated pairs $P^+_{700}A^-_1$ in PS I have been the subject of considerable research.[44, 121, 125–130] It was found that the shape of the dipolar doublets in the Fourier transformed ESEEMs of these systems (see Fig. 9) is similar to the theoretical shape, *i.e.*, these doublets are nearly unbroadened due to other interactions (see Fig. 3). Here, spectral lines are much narrower than in the spectra of similar pairs in bacterial RC or in the reaction centre of PS II (see below). Temperature dependence was also not observed for this spectrum. Small linewidths allowed the distance in the pair to be determined with record (for this range) accuracy, namely, 25.4 ± 0.3 Å.[44, 121] Nearly the same results were obtained in another study.[125] A decrease in r compared to the bacterial RC must be pointed out.

This accuracy also nearly corresponds to the width of the distance distribution in the pair. So narrow distribution for rather long distances seems to be non-trivial. It should be emphasised that the case in point is an amorphous system ($\sim 60\%$ of the total volume is occupied by glycerol, a cryoprotector, which facilitates a low-temperature glass transition). This means that large biomolecules in an amorphous environment can exhibit a high level of structural organisation in the nanometre range of distances.

Studies of reaction centres in which phylloquinone was replaced by various synthetic quinones showed [125, 128, 129] that the distances in RPs in these systems remained constant within the limits of experimental error. This means that synthetic quinones are incorporated at the same binding site as the native quinones. From the EPR spin polarisation data [93] it follows that native and synthetic quinones are oriented in different way. The same distances in these two cases mean that the operation of A_1 as electron acceptor is independent of the binding direction of quinone.[128]

Single crystals of the reaction centre of PS I (symmetry group $P6_3$, two PS I trimers in the unit cell) were studied.[127] Rotation of the crystal revealed a strong orientation dependence of the dipolar doublet, which allowed determination of the orientation of the axis connecting both particles in the pair. The angle was $27 \pm 5^\circ$ relative to the c crystallographic axis and its projection on the *ab* plane is parallel to the a axis.

The results obtained permitted a quite correct determination of two possible positions of phylloquinone A_1 in the electron transfer chain, which appeared to be related by pseudo-C_2 symmetry of chlorophyll cofactors. This was used in the interpretation of X-ray scattering data.[131]

A study of oriented membranes [130] showed that the angle between the direction of the $P_{700}A_1$ pair and the normal to the membrane is $24 \pm 4^\circ$. Based on these results and X-ray scattering data, the direction of electron transfer in RC was suggested.

3. The reaction centre of PS II

Absorption of a light quantum in PS II produces a $P^+_{680}Q^-_A$ radical pair (see Refs 130, 132–134). The width and shape of rather broad lines observed in experiments depend on the sample preparation procedure.[132] If the linewidths were markedly different from the theoretical values, the presence of two different types of pairs with the distances between paramagnetic centres ranging from 26 to 29 Å was assumed.[132] The distances in the pair obtained in other cases were $r = 27.4 \pm 0.3$ Å,[130, 133] 27.2 ± 1 Å,[132] 27.7 ± 0.7 Å.[134] As can be seen, these results are in good agreement with one another, although one study [132] was carried out at 80 K and other studies near room temperature.[133, 134] In respect of a large linewidth the accuracy of measurements reported in Refs 130 and 133 seems to be overestimated.

The angle between the normal to the membrane and the axis of the $P^+_{680}Q^-_A$ pair in oriented membranes was found to be $21 \pm 5^\circ$.[130]

Transformation of the dipolar doublet with an increase in the delay after application of a laser pulse with the characteristic time of the order of 1 ms was reported.[133, 134] This can be explained by the reduction of P_{680} tyrosine Y_Z with the formation of the $Y^{ox}_Z Q^-_A$ pair. Analysis of the dipolar doublet for this pair revealed a distance of 34 ± 1 Å.[134]

4. The Kleinfeld effect

The kinetics of back recombination of the $P^+_{870}Q^-_A$ and $P^+_{870}Q^-_B$ pairs in the reaction centres of purple bacteria differ significantly depending on whether the sample was frozen in the light or in the dark.[135] It is believed that this is due to photo-induced structural changes. X-Ray studies of samples frozen in the light or in the dark were reported.[136] In the latter case, the $P^+_{870}Q^-_B$ pairs were produced. Q^-_B was found to be shifted by 5 Å from the fixed position of the neutral molecule Q_A.

Comparative out-of-phase ESE investigations of the $P^+_{870}Q^-_A$ pairs in the samples frozen in the light or in the dark were reported. No changes in the distance were detected in study [137] while a possible increase in the distance by 0.4 ± 0.2 Å was pointed out in another study.[138] In this case the higher accuracy of measurements was due to the fact that two spectra with practically identical shapes were compared. However, the value determined was found to be too small to explain the Kleinfeld effect by changes in the distance between the P_{870} and Q_A cofactors. Probably, the reason consists in the motion of some polar groups of the molecules involved in charge transfer.

5. Temperature dependence of the supramolecular structure of bacterial reaction centres

The dipolar doublets in bacterial RC exhibit marked temperature dependences.[18, 122] Below 100 K the doublets are considerably broadened. This can be attributed to the appearance of a distance distribution. Comparison with the results of model calculations showed that the width of the distribution function increases from ~ 1 to ~ 4 Å as the temperature decreases to 15 K. At $T < 100$ K, the distribution shape is temperature dependent; a hysteresis was observed on temperature variation.

These data point to the low-temperature dynamics of proteins constituting the RC backbone and containing (in this case) the P_{870} and Q_A cofactors under study. Certain indications of the low-temperature protein dynamics were obtained by different methods, *e.g.*, spectral hole 'burning' in optical spectra and photon echo,[139–141] IR echo,[142, 143] single-molecule spectroscopy,[144] Mössbauer spectroscopy, [145] *etc.* However, in all these cases the dynamics were studied in the atomic scale of distances. But the distances in the $P^+_{870}Q^-_A$ pair show that these effects can be co-operative, being governed by the motion of a certain molecular cluster of nanometre size.

A study [146] similar to that reported in Ref. 122 was carried out at temperatures ~ 15 K and below. It was found that lowering the temperature in the range 13–20 K causes a pronounced line narrowing of the dipolar doublet. This is an indication of a more

ordered state on lowering the temperature. A transition from one state to the other becomes fully reversible. Visually, it is similar to transformation of a crystal into a highly viscous liquid (this is also substantiated by the temperature hysteresis mentioned above). Such low-temperature structural transitions were not reported earlier.

This means that the energy landscape of the protein RC involves very low barriers. A photon echo study [139] of myoglobin revealed low barriers (about several tens of Kelvin).

An observable transition must be characterised by some possibility of structural rearrangements in the nearest environment of protein (in the nanometre range of distances). Dynamic heterogeneity in disordered molecular media, which can arise in this range of distances, has been the subject of intensive discussions.[147, 148]

IX. Conclusion

Pulsed EPR spectroscopy methods based on the electron spin echo technique permit investigations of biomolecule conformations, nanostructure of polymers and the supramolecular structure of such complex objects as photosynthetic reaction centres in plants and bacteria. These methods make it possible to determine the distances between paramagnetic fragments ranging from 15 to ~ 100 Å with a high accuracy (*e.g.*, 0.3 Å at $r \approx 25$ Å in studies of spin-correlated radical pairs in PS I). High resolution allows one to obtain information on fine changes in the nanostructure of matter, occurring under the action of external factors. A marked example is provided by the dynamics of the nanostructure of a bacterial photosynthetic reaction centre at cryogenic temperatures.

Basic to the use of these methods is the presence in the system of free radicals or ions that form pairs or clusters. This situation can be realised naturally (in, *e.g.*, photosynthetic reaction centres or in metal-containing biomolecules) or created artificially by introducing spin probes and labels (usually, based on nitroxyl radicals). At present, a wide use of spin labels is due to the development of biochemical methods of site-directed spin labelling.

Many different methods of investigation of the dipole–dipole interaction between paramagnetic centres have been proposed. The choice of a particular method for studying a given system is governed by the width of the signal in the EPR spectrum and by the relaxation times. Other properties of the system, *e.g.*, the possibility of carrying out comparative experiments in the absence of the dipole–dipole interaction can also play a significant role. When choosing a method of investigation, simplicity of theoretical description and the absence of the masking effects produced by other interactions (in particular, electron–nuclear interaction) are of great importance. The best results in studies of nitroxyl biradicals (most widely used systems) are obtained by the PELDOR technique. Conventional two-pulse ESE spectroscopy is more convenient in studies of photoinduced spin-correlated radical pairs.

Recent advances made by researchers from different laboratories point to great prospects for structural studies of complex molecular systems by pulsed EPR spectroscopy.

The author of this review expresses his gratitude to academician Yu D Tsvetkov for his interest in this study and helpful discussions. This work was financially supported by the Russian Foundation for Basic Research (Project No. 02-03-32022), the NWO (Project No. 047.009.008), the CRDF (Project NO-008-X1), the Siberian Branch of the Russian Academy of Sciences (in the framework of the complex interdisciplinary Project No. 36) and the Grant for support of scientific schools (NSh 919.2003.3).

References

1. J Drenth *Principles of Protein X-ray Crystallography* (New York: Springer, 1994)
2. W Kühlbrandt, D W Wang, Y Fujiyoshi *Nature (London)* **367** 614 (1994)
3. S De Feyter, F C De Schryver *Chem. Soc. Rev.* **32** 393 (2003)
4. A A Shakhatuni, A G Shakhatuni *Usp. Khim.* **71** 1132 (2002) [*Russ. Chem. Rev.* **71** 1005 (2002)]
5. O Kratky, O Glatter (Eds) *Smaller Angle X-ray Scattering* (London: Academic Press, 1982)
6. J S Higgins, H C Benoit *Polymers and Neutron Scattering* (Oxford: Clarendon Press, 1994)
7. P Wu, L Brand *Anal. Biochem.* **218** 1 (1994)
8. O E Yakimchenko, Ya S Lebedev *Usp. Khim.* **47** 1018 (1978) [*Russ. Chem. Rev.* **47** 531 (1978)]
9. K M Salikhov, A G Semenov, Yu D Tsvetkov *Elektronnoe Spinovoe Ekho i Ego Primenenie* (Electron Spin Echo and Its Application) (Nauka: Novosibirsk, 1976)
10. A Schweiger, G Jeschke *Principles of Pulsed Electron Paramagnetic Resonance* (Oxford: Oxford Universuty Press, 2001)
11. V F Yudanov, K M Salikhov, G M Zhidomirov, Yu D Tsvetkov *Teor. Eksp. Khim.* **5** 663 (1969) [a]
12. A D Milov, K M Salikhov, M D Shchirov *Fiz. Tv. Tela* **23** 975 (1981) [b]
13. A D Milov, A B Ponomarev, Yu D Tsvetkov *Chem. Phys. Lett.* **110** 67 (1984)
14. V V Kurshev, A M Raitsimring, Yu D Tsvetkov *J. Magn. Reson.* **81** 441 (1989)
15. S Saxena, J H Freed *Chem. Phys. Lett.* **251** 102 (1996)
16. P P Borbat, J H Freed *Chem. Phys. Lett.* **313** 145 (1999)
17. G Jeschke, M Pannier, A Godt, H W Spiess *Chem. Phys. Lett.* **331** 243 (2000)
18. S A Dzuba, P Gast, A J Hoff *Chem. Phys. Lett.* **236** 595 (1995)
19. P P Borbat, V M Berdnikov, A D Milov, Yu D Tsvetkov *Fiz. Tv. Tela* **19** 1080 (1977)
20. S A Dzyuba, A M Raitsimring, Yu D Tsvetkov *Teoret. eksperim. khimiya* **14** 193 (1978)
21. S A Dzuba, Y Kodera, H Hara, A Kawamori *J. Magn. Reson. A* **102** 257 (1993)
22. L V Kulik, S A Dzuba, I A Grigoryev, Yu D Tsvetkov *Chem. Phys. Lett.* **343** 315 (2001)
23. S A Dzuba, A Kawamori *Concep. Magn. Reson.* **8** 49 (1996)
24. A D Milov, A G Maryasov, Yu D Tsvetkov *Appl. Magn. Reson.* **15** 107 (1998)
25. S S Eaton, G R Eaton, in *Distance Measurements in Biological Systems by EPR Biological Magnetic Resonance* Vol. 19 (Eds G R Eaton, S S Eaton, L J Berliner) (New York: Kluwer Academic, Plenum, 2000) p. 348
26. P Borbat, J H Freed, in *Distance Measurements in Biological Systems by EPR Biological Magnetic Resonance* Vol. 19 (Eds G R Eaton, S S Eaton, L J Berliner) (New York: Kluwer Academic, Plenum, 2000) p. 383
27. A Raitsimring, in *Distance Measurements in Biological Systems by EPR Biological Magnetic Resonance* Vol. 19 (Eds G R Eaton, S S Eaton, L J Berliner) (New York: Kluwer Academic, Plenum, 2000) p. 461
28. K V Lakshmi, G W Brudvig, in *Distance Measurements in Biological Systems by EPR Biological Magnetic Resonance* Vol. 19 (Eds G R Eaton, S S Eaton, L J Berliner) (New York: Kluwer Academic, Plenum, 2000) p. 513
29. S A Dzuba, A J Hoff, in *Distance Measurements in Biological Systems by EPR Biological Magnetic Resonance* Vol. 19 (Eds G R Eaton, S S Eaton, L J Berliner) (New York: Kluwer Academic, Plenum, 2000) p. 569
30. T Prisner, M Rohrer, F MacMillan *Annu. Rev. Phys. Chem.* **52** 279 (2001)
31. W Lubitz, F Lendzian, R Bittl *Acc. Chem. Res.* **35** 313 (2002)
32. G Jeschke *Chem. Phys. Chem.* **3** 927 (2002)
33. G Jeschke *Macromol. Rapid Commun.* **23** 227 (2002)

34. Yu D Tsvetkov, in *EPR: Instrumental Methods, Biological Magnetic Resonance* Vol. 21 (Eds C J Bender, L J Berliner) (New York: Kluwer Academic, Plenum, 2004) p. 385
35. L V Kulik, S A Dzyuba *Zh. Strukt. Khim.* **45** 313 (2004) [c]
36. C R Timmel, C E Fursman, A J Hoff, P J Hore *Chem. Phys.* **226** 271 (1998)
37. M Pannier, S Veit, A Godt, G Jeschke, H W Spiess *J. Magn. Reson.* **142** 331 (2000)
38. L V Kulik, Yu A Grishin, S A Dzuba, I A Grigoryev, S V Klyatskaya, S F Vasilevsky, Yu D Tsvetkov *J. Magn. Reson.* **157** 61 (2002)
39. A A Dubinskii, Yu A Grishin, A N Savitsky, K Mobius *Appl. Magn. Reson.* **22** 369 (2002)
40. A Weber, O Schiemann, B Bode, T Prisner *J. Magn. Reson.* **157** 277 (2002)
41. K M Salikhov, Yu E Kandrashkin, A K Salikhov *Appl. Magn. Reson.* **3** 199 (1992)
42. J Tang, M C Thurnauer, J R Norris *Chem. Phys. Lett.* **219** 283 (1994)
43. J Tang, M C Thurnauer, A Kubo, H Hara, A Kawamori *J. Chem. Phys.* **106** 7471 (1997)
44. R Bittl, S G Zech *J. Phys. Chem. B* **101** 1429 (1997)
45. S A Dzuba *Chem. Phys. Lett.* **278** 333 (1997)
46. I V Borovykh, L V Kulik, S A Dzuba, A J Hoff *Chem. Phys. Lett.* **338** 173 (2001)
47. A V Kulikov, G I Likhtenshtein *Adv. Mol. Relax. Interact. Process* **10** 47 (1977)
48. R W Quine, S S Eaton, G R Eaton *Rev. Sci. Instrum.* **63** 4252 (1992)
49. S A Dzuba, A M Raitsimring, Yu D Tsvetkov *Chem. Phys.* **44** 357 (1979)
50. L V Kulik, S V Paschenko, S A Dzuba *J. Magn. Reson.* **159** 237 (2002)
51. L V Kulik, I A Grigor'ev, E S Salnikov, S A Dzuba, Yu D Tsvetkov *J. Phys. Chem. A* **107** 3692 (2003)
52. Y Kodera, S A Dzuba, H Hara, A Kawamori *Biochim. Biophys. Acta* **1186** 91 (1994)
53. I V Borovykh, L V Kulik, S A Dzuba, A J Hoff *J. Phys. Chem. B* **106** 12066 (2002)
54. L V Kulik, I V Borovykh, P Gast, S A Dzuba *J. Magn. Reson.* **162** 423 (2003)
55. A D Milov, A B Ponomarev *Zh. Strukt. Khim.* **25** 51 (1984) [c]
56. R G Larsen, D J Singel *J. Chem. Phys.* **98** 5134 (1993)
57. A Yu Pusep, N V Shokhirev *Opt. Spektrosk.* **57** 792 (1984) [d]
58. G Jeschke, A Koch, U Jonas, A Godt *J. Magn. Reson.* **155** 72 (2002)
59. V Pfannebecker, H Klos, M Hubrich, T Volmer, A Heuer, U Wiesner, H W Spiess *J. Phys. Chem.* **100** 13428 (1996)
60. E Narr, A Godt, G Jeschke *Angew. Chem., Int. Ed.* **41** 3907 (2002)
61. A D Milov, Yu D Tsvetkov *Appl. Magn. Reson.* **12** 495 (1997)
62. W L Hubbell, C Altenbach, C M Hubbell, H G Kworana *Adv. Protein Chem.* **63** 288 (2003)
63. H J Steinhoff, B Suess *Methods* **29** 188 (2003)
64. J C McNulty, G L Millhauser, in *Distance Measurements in Biological Systems by EPR Biological Magnetic Resonance* Vol. 19 (Eds G R Eaton, S S Eaton, L J Berliner) (New York: Kluwer Academic, Plenum, 2000) p. 277
65. A D Milov, A G Maryasov, Yu D Tsvetkov, J Raap *Chem. Phys. Lett.* **303** 135 (1999)
66. A D Milov, A G Mar'yasov, R I Samoilova, Yu D Tsvetkov, Ya Raap, V Monako, F Formadzhio, M Krisma, K Toniolo *Dokl. Akad. Nauk* **370** 265 (2000) [e]
67. A D Milov, Yu D Tsvetkov, F Formaggio, M Crisma, C Toniolo, J Raap *J. Am. Chem. Soc.* **123** 3784 (2001)
68. P Hanson, G Martinez, G L Millhauser *J. Am. Chem. Soc.* **118** 271 (1996)
69. V Monaco, F Formaggio, M Crisma, C Toniolo, P Hanson, G Millhauser, C Cegre, J Deschamps, J Flippen-Anderson *Bioorg. Med. Chem.* **7** 119 (1999)
70. D Anderson, P Hanson, J McNulty, G Millhauser, V Monako, F Formaggio, M Crisma, C Toniolo *J. Am. Chem. Soc.* **121** 6919 (1999)
71. V Monako, F Formaggio, M Crisma, C Toniolo, P Hanson, G L Millhauser *Biopolymers* **50** 239 (1999)
72. P P Borbat, H S McHaourab, J H Freed *J. Am. Chem. Soc.* **124** 5304 (2002)
73. O Schiemann, A Weber, T E Edwards, T Prisner, S T Sigurdsson *J. Am. Chem. Soc.* **125** 3434 (2003)
74. M Bennati, A Weber, J Aubnic, D L Perlstein, J Robblee, J Stabber *J. Am. Chem. Soc.* **125** 14988 (2003)
75. M H Rakowsky, K M More, A V Kulikov, G R Eaton, S S Eaton *J. Am. Chem. Soc.* **117** 2049 (1995)
76. M H Rakowsky, A Zecevic, G R Eaton, S S Eaton *J. Magn. Reson.* **131** 97 (1998)
77. V Budker, J L Du, M Seiter, G R Eaton, S S Eaton *Biophys. J.* **68** 2531 (1995)
78. M Seiter, V Budker, J L Du, G R Eaton, S S Eaton *Inorg. Chim. Acta* **273** 354 (1998)
79. C Elasser, M Brecht, R Bittl *J. Am. Chem. Soc.* **124** 12 606 (2002)
80. R Codd, A V Astashkin, A Pacheco, A M Raitsimring, J H Enemark *J. Biol. Inorg. Chem.* **7** 338 (2002)
81. A D Milov, Yu D Tsvetkov, F Formaggio, M Crisma, C Toniolo, J Raap *J. Am. Chem. Soc.* **122** 3843 (2000)
82. A D Milov, Yu D Tsvetkov, F Formaggio, M Crisma, C Toniolo, G L Millhauser, J Raap *J. Phys. Chem. B* **105** 11 206 (2001)
83. A D Milov, Yu D Tsvetkov, J Raap *Appl. Magn. Reson.* **19** 215 (2000)
84. A D Milov, Yu D Tsvetkov, E Yu Gorbunova, L G Mustaeva, T V Ovchinnikova, J Raap *Biopolymers* **64** 326 (2002)
85. A D Milov, Yu D Tsvetkov, F Formaggio, S Oancea, C Toniolo, J Raap *J. Phys. Chem. B* **107** 13719 (2003)
86. A D Milov, Yu D Tsvetkov, F Formaggio, M Crisma, C Toniolo, J Raap *J. Peptide Sci.* **9** 690 (2003)
87. S Schlick *Ionomers: Characterization Theory and Applications* (New York: CRC Press, 1996)
88. A Eisenberg, J-S Kim *Introduction to Ionomers* (New York: Wiley, Interscience, 1998)
89. M Pannier, V Schadler, M Schops, U Wiesner, G Jeschke, H W Spiess *Macromolecules* **33** 7812 (2000)
90. M Pannier, M Schops, V Schadler, U Wiesner, G Jeschke, H W Spiess *Macromolecules* **34** 5555 (2001)
91. V Schadler, A Frank, U Wiesner, H W Spiess *Macromolecules* **30** 3832 (1997)
92. A J Hoff, J Deisenhofer *Phys. Rep.* **287** 1 (1997)
93. A van der Est *Biochem. Biophys. Acta* **1507** 212 (2001)
94. R Bittl, S G Zech *Biochem. Biophys. Acta* **1507** 194 (2001)
95. W Lubitz, F Lendrian, R Bittl *Acc. Chem. Res.* **35** 3313 (2002)
96. J Deisenhofer, O Epp, K Miki, R Huber, H Michel *J. Mol. Biol.* **180** 385 (1984)
97. J P Allen, G Feher, T O Yeates, H Komiya, D C Rees *Proc. Natl. Acad. Sci. USA* **84** 5730 (1987)
98. H Komiya, T O Yeates, D C Rees, J P Allen, J Feher *Proc. Natl. Acad. Sci. USA* **85** 9012 (1988)
99. C-H Chang, O El-Kabbani, D Tiede, J Norris, M Schiffer *Biochemistry* **30** 5352 (1991)
100. N Krauss, W-D Schubert, O Klukas, P Fromme, H T Witt, W Saenger *Nat. Struct. Biol.* **3** 965 (1996)
101. A Zouni, H T Witt, J Kern, P Fromme, N Krauss, W Saenger, P Orth *Nature (London)* **409** 739 (2001)
102. N Kamiya, J R Shen *Proc. Natl. Acad. Sci. USA* **100** 98 (2003)
103. J Xiong, S Subramaniam *Govindjee, Photosynth. Res.* **3** 229 (1998)
104. B Kok, B Forbush, M McGloin *Photochem. Photobiol.* **11** 457 (1970)
105. J Limburg, V A Szalai, G W Brudvig *J. Chem. Soc., Dalton Trans.* **9** 1353 (1999)
106. H Hara, A Kawamori *Appl. Magn. Reson.* **13** 241 (1997)
107. Y Kodera, H Hara, A V Astashkin, A Kawamori, T A Ono *Biochim. Biophys. Acta* **1232** 43 (1995)
108. D Koulouglioris, R H Schweitzer, G V Brudvig *Biochemistry* **36** 9735 (1997)
109. K V Lakshmi, S S Eaton, G R Eaton, H A Frank, G W Brudvig *J. Phys. Chem. B* **102** 8327 (1998)
110. J M Peloquin, K A Campbell, R D Britt *J. Am. Chem. Soc.* **120** 6840 (1998)
111. P Dorlet, M Di Valentin, G T Babcock, J L McCracken *J. Phys. Chem. B* **102** 8239 (1998)

112. K V Lakshmi, S S Eaton, G R Eaton, G W Brudvig *Biochemistry* **38** 12758 (1999)
113. H Hara, A Kawamori, A V Astashkin, T Ono *Biochim. Biophys. Acta* **1276** 140 (1996)
114. A V Astashkin, Y Kodera, A Kawamori *Biochim. Biophys. Acta* **1187** 89 (1994)
115. A V Astashkin, H Hara, A Kawamori *J. Chem. Phys.* **108** 3805 (1998)
116. M Tonaka, A Kawamori, H Hara, A V Astashkin *Appl. Magn. Reson.* **19** 141 (2000)
117. K Shigemori, H Hara, A Kawamori, K Akabori *Biochim. Biophys. Acta.* **1363** 187 (1998)
118. D Koulougliotis, X-S Tang, B A Diner, G W Brudwig *Biochemistry* **34** 2850 (1995)
119. M C Thurnauer, J R Norris *Chem. Phys. Lett.* **76** 557 (1980)
120. M C Thurnauer, C Clark *Photochem. Photobiol.* **40** 381 (1984)
121. S G Zech, W Lubitz, R Bittl *Ber. Bunsen-Ges. Phys. Chem.* **100** 2041 (1996)
122. S A Dzuba, P Gast, A J Hoff *Chem. Phys. Lett.* **268** 273 (1997)
123. A T Gardiner, S G Zech, F MacMillan, H Kass, R Bittl, E Schlodder, F Lendzian, W Lubitz *Biochemistry* **38** 11773 (1999)
124. R Lancaster, H Michel *Structure* **5** 1339 (1997)
125. S A Dzuba, H Hara, A Kawamori, M Iwaki, S Itoh, Yu D Tsvetkov *Chem. Phys. Lett.* **264** 238 (1997)
126. H Hara, J Tang, A Kawamori, S Itoh, M Iwaki *Appl. Magn. Reson.* **14** 367(1998)
127. R Bittl, S G Zech, P Fromme, H T Witt, W Lubitz *Biochemistry* **36** 12001 (1997)
128. S G Zech, A J van der Est, R Bittl *Biochemistry* **36** 9774 (1997)
129. M Iwaki, S Itoh, H Hara, A Kawamori *J. Phys. Chem. B* **102** 10440 (1998)
130. T Yoshii, H Hara, A Kawamori, K Akabori, M Iwaki, S Itoh *Appl. Magn. Reson.* **16** 565 (1999)
131. W-D Schubert, O Klukas, N Krauss, W Saenger, P Fromme, H T Witt *J. Mol. Biol.* **272** 741 (1997)
132. H Hara, S A Dzuba, A Kawamori, K Akabori, T Tomo, K Satoh, M Iwaki, S Itoh *Biochim. Biophys. Acta* **1322** 77 (1997)
133. S G Zech, J Kurreck, H J Eckert, G Renger, W Lubitz, R Bittl *FEBS Lett.* **414** 454 (1997)
134. S G Zech, J Kurreck, G Renger, W Lubitz, R Bittl *FEBS Lett.* **442** 79 (1999)
135. D Kleinfeld, M Y Okamura, G Feher *Biochemistry* **23** 5780 (1984)
136. M H B Stowell, T M McPhillips, D C Rees, S M Soltis, E Abresch, G Feher *Science* **276** 812 (1997)
137. S G Zech, R Bittl, A T Gardiner, W Lubitz *Appl. Magn. Reson.* **13** 517 (1997)
138. I V Borovykh, S A Dzuba, I I Proskuryakov, P Gast, A J Hoff *Biochim. Biophys. Acta* **1363** 182 (1998)
139. D T Leeson, D A Wiersma, K Frisch, J Friedrich *J. Phys. Chem. B* **101** 6331 (1997)
140. F T H den Hartog, C van Papendrecht, U Storkel, S Volker *J. Phys. Chem. B* **103** 1375 (1999)
141. J Schlichter, J Friedrich, L Herenyi, J Fidy *Biophys. J.* **80** 2011 (2001)
142. K D Rector, J R Engholm, C W Rella, J R Hill, D D Dlott, M D Fayer *J. Phys. Chem. A* **103** 2381 (1999)
143. M D Fayer *Annu. Rev. Phys. Chem.* **52** 315 (2001)
144. C Tietz, F Jelezko, U Gerken, S Schuler, A Schubert, H Rogl, J Wrachtrup *Biophys. J.* **81** 556 (2001)
145. F Parak, K Achterhold *Hyperfine Interact.* **123** 825 (1999)
146. I V Borovykh, L V Kulik, P Gast, S A Dzuba *Chem. Phys.* **294** 433 (2003)
147. H Sillescu *J. Non-Cryst. Solids* **243** 81 (1999)
148. M D Ediger *Annu. Rev. Phys. Chem.* **51** 99 (2000)

[a] — *Theor. Exp. Chem. (Engl. Transl.)*
[b] — *Phys. Solid State (Engl. Transl.)*
[c] — *Russ. J. Struct. Chem. (Engl. Transl.)*
[d] — *Opt. Spectroscop. (Engl. Transl.)*
[e] — *Dokl. Chem. (Engl. Transl.)*